

TITLE PAGE

G protein pre-assembly rescues efficacy of W^{6.48} toggle mutations in neuropeptide Y₂ receptor

Anette Kaiser, Caroline Hempel, Lizzy Wanka, Mario Schubert, Heidi E. Hamm, and Annette G. Beck-Sickinger

Faculty of Biosciences, Pharmacy and Psychology, Institute of Biochemistry, Leipzig University, Bruederstrasse 34, 04103 Leipzig, Germany. (A.K., C.H., L.W., M.S., A.G.B.-S.)
Department of Pharmacology, Vanderbilt University Medical Center, Nashville, TN 37232-6600, USA. (A.K., C.H., H.E.H)

RUNNING TITLE PAGE

Effector coupling of Y₂ receptor and W^{6.48} toggle mutations

Corresponding author:

Dr. Anette Kaiser

Institute of Biochemistry, Brüderstraße 34, 04103 Leipzig (Germany)

Phone: +49 341 341 9736737

Fax: +49 341 341 9736909

anette.kaiser@uni-leipzig.de

42 pages

5 tables

8 figures

66 references

Abstract: 249 words

Introduction: 716 words

Discussion: 1489 words

Non-standard abbreviations:

BRET, bioluminescence resonance energy transfer; **CRE**, cAMP-response element; **ECL**, extracellular loop; **ER**, endoplasmic reticulum; **GPCR**, G protein-coupled receptor; **Nal**, naphthylalanine; **NPY**, neuropeptide Y; **TM**, transmembrane helix; **Y₂R**, neuropeptide receptor subtype 2

ABSTRACT

Ligand binding and pathway-specific activation of G protein-coupled receptors (GPCRs) is currently study with great effort. Individual answers may depend on the nature of the ligands and the effector pathway. Recently, we have presented a detailed model of NPY bound to the Y₂R (Kaiser et al., 2015). Accordingly, the C-terminal part of the peptide binds deeply in the transmembrane bundle and brings the side chain of the most essential Y³⁶ in close proximity to W^{6.48}. Here, we investigate the role of this interaction for ligand binding and activation of this receptor. BRET sensors were used for detailed investigation of effector coupling, and led to the identification of pre-assembly of the Y₂R-G_i complex. It further confirmed ligand-dependent recruitment of arrestin3. Using equally sensitive readouts for G_i activation and arrestin recruitment as well as quantification with operational models of agonism allowed us to identify a strong inherent bias for G_i activation over arrestin3 recruitment for the wild type receptor. By systematic mutagenesis, we found that W^{6.48} does not contribute to the binding affinity, but acts as allosteric connector to couple ligand binding to G_i-activation and arrestin3 recruitment. However, even mutagenesis to a small threonine did not lead to a complete loss of signaling. Interestingly, signaling was restored to wild type levels by ligands that contain a naphthylalanine as the C-terminal residue instead of Y³⁶. Steric and polar contributions of W^{6.48} for the activation of the receptor are discussed in the context of different mechanisms of G protein coupling and arrestin recruitment.

INTRODUCTION

Within the last decades, the view of G protein coupled receptors (GPCRs) has changed from simple on/off signal transduction switches to multifaceted relays with tight spatiotemporal regulation and multidimensional signaling through various intracellular effectors. Specifically, the discovery of functional selectivity that addresses only a subset of possible effectors for a given receptor holds great promises for tailored pharmaceutical interventions (Rajagopal *et al.*, 2010; Khoury *et al.*, 2014). Only a small fraction of the overall 800 members are currently targeted by pharmaceuticals, yet this accounts for at least 30% of all marketed drugs (Hopkins and Groom, 2002; Garland, 2013). Thus, it remains a major task to further advance our understanding in finding common and individual themes of GPCR regulation, and particularly activation, to aid rational drug design.

Peptide-binding receptors make up a significant fraction of the rhodopsin-family, and are attractive targets for instance for the treatment of obesity and pain (Wu *et al.*, 2017). Their binding mode and activation, however, has long remained enigmatic (Schwartz and Rosenkilde, 1996). In recent years, crystallographic snapshots could be obtained for some of these receptors, revealing great variability of the binding pockets with respect to charge distribution and depth (Krumm and Grisshammer, 2015; Wu *et al.*, 2017). Most of these structures, however, were obtained in complex with non-peptidic or peptidic antagonists, and the neurotensin receptor 1 (NTSR1) remains the only receptor co-crystallized with its peptidic agonist (White *et al.*, 2012; Egloff *et al.*, 2014; Krumm *et al.*, 2015, 2016). Nonetheless, the entity of the structures obtained so far suggests that also peptide-activated GPCRs bind to the suggested common binding crevice, similar to the well-studied GPCRs with much smaller adrenergic or aminergic ligands (Venkatakrisnan *et al.*, 2013).

We have recently presented a model of the neuropeptide Y₂ receptor bound to its agonist NPY¹³⁻³⁶ by combining NMR, mutagenesis, and molecular modeling (Kaiser *et al.*, 2015). In line with recent crystallographic structures, we demonstrated that despite of its size, neuropeptide Y binds deeply in the transmembrane bundle guided by hydrophobic contacts of its amphipathic helix to the second extracellular loop, and unwinds its five C-terminal residues

from the α -helix to make optimal contacts in the deep binding pocket (Kaiser *et al.*, 2015). The Y₂R is part of the neuropeptide Y multiligand-multireceptor family, and is activated by the 36 amino acid C-terminally amidated neuropeptide Y and peptide YY as well as N-terminally truncated peptide variants (Pedragosa-Badia *et al.*, 2013). It couples to the inhibitory family of G proteins (G_{i/o}) (Michel *et al.*, 1998), and has also been shown to recruit arrestin3 (Berglund *et al.*, 2003; Kilpatrick *et al.*, 2010; Walther *et al.*, 2010; Gimenez *et al.*, 2014). The individual contributions of these pathways for physiological function (anorectic effects, neuroprotection, vascularization), however, have not yet been characterized (Babilon *et al.*, 2013). Thus, detailed understanding of the prerequisites for binding and activation of either signaling pathway will help to develop (pathway) specific ligands, and rationalize antagonistic and agonistic ligand properties.

Interestingly, in the Y₂R model (Kaiser *et al.*, 2015) the side chain of the essential Y³⁶ of the ligand is pointing towards W^{6.48} of the receptor (nomenclature according to (Ballesteros and Weinstein, 1995)). This position had been proposed as part of a global toggle-switch mechanism in GPCR activation (Schwartz *et al.*, 2006; Holst *et al.*, 2010; Katritch *et al.*, 2013), and exchange of this residue leads to a complete loss of G_q activation of several receptors (Holst *et al.*, 2010), including two peptide-activated receptors.

Thus, we investigated this position for binding and activation of the Y₂R. We systematically mutated the tryptophan side chain and analyzed coupling of G_i, a chimeric G_{iq} protein as well as arrestin3 by second messenger assays and live-cell fluorescence microscopy, as well as by bioluminescence energy transfer (BRET). The use of BRET sensors allowed for a detailed investigation of the effector coupling mechanism, and revealed significant pre-assembly of Y₂R-G_i in the absence of ligand. Mutagenesis of W^{6.48} had detrimental effects for all signaling pathways, but mutants still displayed significant activity even with a small threonine side chain. Furthermore, signaling was restored close to wild type levels by ligands designed to harbor a naphthylalanine as the C-terminal residue. Steric and polar contributions of W^{6.48} for activation of the receptor are discussed in the context of different mechanisms of G protein coupling and arrestin recruitment.

MATERIALS and METHODS

Peptide synthesis

NPY (H-YPSKPDNPGEDAPAEDLARYYSALRHYINLITRQRY-NH₂) and C-terminally modified analogues were generated by Fmoc/*tert*-butyl solid phase peptide synthesis in 15 μ mol scale as reported (Kaiser *et al.*, 2015). For the synthesis of the C-terminally modified NPY variants, Fmoc-1NaI³⁶-OH (Iris Biotech, Marktredwitz, Germany) or Fmoc-2NaI³⁶-OH, respectively, were loaded manually on Rink amide resin (15 μ mol) instead of Fmoc-Tyr(*tert*-butyl)-OH by using 5 equivalents (75 μ mol) each of amino acid, and coupling reagents 1-hydroxy-benzotriazole and diisopropylcarbodiimide in *N,N*-dimethylformamide. Coupling of the first amino acid was performed over night, followed by automated elongation (repetitive cycles of Fmoc deprotection, activation and coupling of the next amino acid) in a Syro II peptide synthesizer (MultiSynTech, Witten, Germany). Peptides were cleaved from the resin by using trifluoroacetic acid/thioanisole/thiocresol (90/5/5, v/v/v) for 2 h, and precipitated using ice cold diethyl ether. Identity of the peptides was confirmed by MALDI-ToF mass spectrometry (Ultraflex III MALDI ToF/ToF, Bruker, Billerica, USA), and the peptides were purified to > 95% as reported (Kaiser *et al.*, 2015).

Generation of plasmids

The coding sequence of human Y₂R was cloned into pEYFP_N1 expression vector (Clontech, Mountain View, USA) as described (Dinger *et al.*, 2003). Mutations at position W²⁸¹ (W^{6.48} according to Ballesteros and Weinstein nomenclature (Ballesteros and Weinstein, 1995)) were introduced by using QuikChange mutagenesis (Stratagene, Agilent, Santa Clara, USA). For BRET experiments with Venus-tagged G α -proteins (see below), Y₂R variants were fused to a modified Renilla luciferase (Rluc8 (Loening *et al.*, 2006)) in pcDNA3 vector (Gimenez *et al.*, 2014). Bovine arrestin3 was tagged at its N-terminus with Rluc8 or Venus (Vishnivetskiy *et al.*, 2011) in pcDNA3 vector, or mCherry-arr3 (Walther *et al.*, 2010) as described.

Since N- and C-terminal regions are critical for receptor recognition and functionality of G α -subunits (Oldham and Hamm, 2008), we introduced Rluc8 or a monomeric variant (A²⁰⁶K)

(Zacharias *et al.*, 2002) of the Venus fluorophore (Nagai *et al.*, 2002) into the helical domain next to M¹¹⁹ (G α_{i1})/P¹²⁷ (G α_q / chimeric G $\alpha_{\Delta 6q14myr}$) by using a Ser-Gly-Gly-Gly-Gly-Ser-linker. Human G α_{i1} in pcDNA3 was obtained from UMR cDNA Ressource Center (Rolla, USA), and chimeric G $\alpha_{\Delta 6q14myr}$ (Kostenis *et al.*, 2005) was kindly provided by E. Kostenis. Cloning was performed by PCR overlap extension using *Pfu* Polymerase and fusion protein was inserted into pcDNA3 vector by *HindIII* (5') and *XhoI* (3') restriction sites (all enzymes by Fermentas Thermo Scientific, Waltham, USA). Construct identity was verified by Sanger dideoxy sequencing.

¹²⁵I-PYY binding assays

Binding assays were performed with membrane preparations of transiently transfected HEK293 cells. Membranes were prepared according to Beck-Sickinger *et al.* (Beck-Sickinger *et al.*, 1994) with some modification. Cells were detached by washing with Ca²⁺/Mg²⁺-free phosphate buffered saline (PAA, Pasching, Austria), collected by centrifugation at 800 x g for 10 min, frozen in liquid nitrogen, and stored at -80 °C. Cell pellets were taken up in 50 mM Tris-Cl buffer pH 7.5 (containing protease inhibitors: 50 μ M Pefabloc SC (Fluka, Sigma-Aldrich, St. Louis, USA) and homogenized 25 times with a Potter (Potter S, B. Braun International) under ice cooling. The suspension was then centrifuged at 4 °C, 7400 x g for 10 min to remove cell debris, and the supernatant was centrifuged at 4 °C, 18500 x g for 60 min. The resulting pellet containing the microsomal membrane preparation was resuspended in 25 mM HEPES, 25 mM CaCl₂, 1 mM MgCl₂, pH 7.4, containing 50 μ M Pefabloc, and homogenized again 25 times in an ice bath. The suspension was centrifuged at 4°C, 18500 x g for 120 min, and the pellet was resuspended in HEPES buffer w/o protease inhibitors for determination of protein concentration. Subsequently, Pefabloc was added to a final concentration of 50 μ M, and membrane preparations were stored in aliquots at -80 °C.

¹²⁵I-pPYY was obtained from Perkin Elmer (NEX240, 81.4 TBq/mmol; Waltham, USA). Radioligand binding experiments were performed in 100 μ l total volume in 96 well plates in HEPES/Ca²⁺/Mg²⁺/Pefabloc buffer containing 1% (w/v) bovine serum albumin, using 0.5 μ g

total protein per well. Unspecific binding was measured in the presence of 1 μ M NPY and subtracted from data. Saturation binding experiments were incubated under gentle agitation for 3 h at room temperature. In dissociation experiments, NPY was added to a final concentration of 1 μ M after 3 h. The remaining bound radioactivity was subsequently determined at several time points to obtain an estimate of k_{off} . Assays were terminated by filtration and washing (3x 200 μ l) with ice cold PBS using MicroBeta Filtermat-96 cell harvester (Perkin Elmer, Waltham, USA). Membranes were pre-treated with 0.1% polyethylenimine (w/v) in PBS. Radioactivity was determined by scintillation counting (MicroBeta2, Perkin Elmer, Waltham, USA). Binding assays were performed at least three times independently, and were measured in duplicate.

Inositol phosphate accumulation assay (via chimeric $G\alpha_{\Delta 6qi4myr}$)

For easy and robust readout of receptor activity, a chimeric $G\alpha_{\Delta 6qi4myr}$ protein was co-transfected to redirect the endogenous $G_{i/o}$ signaling of Y receptors to the phospholipase C pathway (Kostenis *et al.*, 2005). A detailed protocol is described elsewhere (Els *et al.*, 2010; Witte *et al.*, 2013). Briefly, COS7 cells transiently transfected with receptor and chimeric $G\alpha_{\Delta 6qi4myr}$ protein were labeled with 2 μ Ci/ml 3 H-myo-inositol (Perkin Elmer, Waltham, USA) in 48 well plate format, stimulated with different concentrations of peptide, and 3 H-inositol phosphates were isolated from cell lysates by anion-exchange chromatography, and measured by liquid scintillation counting. Experiments were performed in duplicate and repeated three times independently.

cAMP assays (via endogenous $G\alpha_i$)

Signal transduction was investigated in a reporter gene assay based on endogenous G_i (OneGlo™ luciferase reporter gene assay, Promega, Madison, USA). Plasmids encoding the receptor mutant (4 μ g) and the luciferase reporter under control of a cAMP response element (CRE) pGL4.29[luc2P/CRE/Hygro] (4 μ g) were co-transfected into 70% confluent HEK293 cells in 6-well plates using Lipofectamine2000™ (Life Technologies, Thermo Fisher Scientific,

Carlsbad, CA, USA) lipofection reagent according to manufacturer's instructions. One day after transfection, cells were re-seeded onto poly-D-lysine coated 96-well plates (white, clear bottom; 125,000 cells/well), and grown for another day. Prior to stimulation, cells were serum-deprived for 1 h, and then stimulated with varying NPY concentrations (10^{-13} M – 10^{-6} M, triplicate each) in the presence 1 μ M forskolin (Sigma-Aldrich, St. Louis, USA) in serum-free medium for 2 h at 37 °C. Cells were then washed once, 30 μ l serum-free medium/well was added and cells were equilibrated to room temperature for 10 min. Subsequently, 30 μ l OneGlo reagent/well (room temperature) was added, and incubated 5 min in the dark before measuring luminescence in a plate reader (Tecan Infinite 200, Tecan, Männedorf, Switzerland).

Fluorescence microscopy

Membrane localization, arrestin3-recruitment, and internalization of Y₂R variants was investigated in live HEK293 cells using an Axiovert Observer Z1 microscope (with Apotome, Plan-Apochromat 63x/1.40 Oil DIC objective; Carl Zeiss, Jena, Germany). HEK293 cells were seeded in μ -slides (Ibidi, Martinsried, Germany), and transiently transfected with Y₂R-eYFP variants +/- mCherry-arrestin3 by using Lipofectamine2000 (1000 ng total DNA/well, 4:1 receptor:arrestin3). One day after transfection, standard cell culture medium (containing 15% fetal calf serum) was changed to serum-reduced OptiMEM (Gibco, Thermo Fisher Scientific, Waltham, USA), and nuclei were stained with Hoechst 33342 (5 μ g/ml final concentration) for 30 min. Cellular localization of receptor and arrestin was assessed before (0 min) and after stimulation with 1 or 10 μ M NPY at 37 °C for the time indicated applying identical exposure time and image processing. Quantification of microscopy images was performed by using ImageJ (Rasband, W.S., U. S. National Institutes of Health, Bethesda, Maryland, USA, <https://imagej.nih.gov/ij/>, 1997-2017). To demonstrate arrestin recruitment, line scans were carried out for stacked images from mCherry (arrestin-3) and eYFP (Y₂R) channel using the reslice function, and values were normalized. Receptor internalization was quantified by determining the mean fluorescence intensity at the plasma membrane with the segmented line

function. Background fluorescence was subtracted. For each condition, at least 12 cells from 4 independent images were analyzed, and the experiment was repeated twice independently.

BRET assays

BRET assays were performed with transiently transfected HEK293 cells. Cells were seeded in 6-well plates and transfected with a gradient of Venus-tagged BRET acceptor at 70% confluence. For arrestin-interaction studies, 4000 ng DNA was transfected per well (100 ng Rluc8-arrestin3, 0-3900 ng Y₂R-eYFP), and the total DNA amount was balanced by empty pcDNA3 vector, using 3 μ l MetafectenePro (Biontex, Munich, Germany) per μ g DNA. For the investigation of G-protein interaction, the total DNA amount was reduced to 1800 ng (200 ng Y₂R-Rluc8, 0-1600 ng G α -Venus). Cells were re-seeded onto white and black poly-D-lysine coated 96-well plates (125,000 cells/well) for measurement of BRET, and direct excitation of Venus to determine expression levels, respectively. Ligand-concentration-response and kinetic experiments were performed at maximal Venus/Rluc8 ratio, i.e. BRET donor saturation. BRET was measured at 37 °C in HBSS buffer supplemented with 25 mM HEPES (pH 7.4; 100 μ l). Cells were pre-incubated with fresh Coelenterazine h (addition of 50 μ l of 16.7 μ M stock solution; final: 4.2 μ M; NanoLight, Pinetop, USA) for 5 min, and stimulated (t = 0 min) with 50 μ l 4x ligand solution (final volume 200 μ l/well). Fluorescence and luminescence were measured in a plate reader (Tecan infinite M 200; Tecan, Männedorf, Switzerland) at the indicated times by using the filter sets Blue1 (luminescence 370-480 nm) and Green1 (fluorescence 520-570 nm). BRET ratio was calculated as ratio of fluorescence and luminescence subtracted by signals of donor-only (Rluc8) transfected cells. NetBRET was determined by subtracting BRET signals of unstimulated cells from ligand-stimulated samples. To determine expression levels of the BRET-acceptor (Venus) in saturation BRET assays, fluorescence was measured by direct excitation (Exc 488(9), Em 530(20)) in black plates and divided by basal luminescence of donor-only transfected cells to calculate F/L ratio (x-axis).

Data analysis

Nonlinear regression analysis was performed with GraphPad Prism 5.03 (GraphPad Software, San Diego, USA). For saturation binding radioligand experiments, specific binding was fit using the one-site binding isotherm (rectangular hyperbola) for the determination of K_D and B_{max} . In displacement binding experiments, each receptor variant was normalized to its own specific binding, and data were analyzed using logistic functions to test for one (one site – fit IC_{50}) or two affinity states (two sites – fit IC_{50}). Kinetic radioligand binding data (k_{off}) were normalized to specific binding at $t=0$ min (100%), and fit using an exponential function for a two-phase decay with shared values for both time constants in the presence/absence of $GTP\gamma S$, but individually for each receptor mutant.

Concentration-response curves of signal transduction (2nd messenger and BRET) experiments were fit with a three-parameter logistic function with fixed Hill slope ($n_H = 1$) to determine EC_{50} and E_{max} values. In addition, concentration-response curves were fit using the operational model of agonism (Black and Leff, 1983) with the built-in function of GraphPad Prism, fixing the E_{max} to the maximal system stimulation and allow for fit of both K_A and τ , as well as direct calculation of ratio $\log(\tau/K_A)$. For second messenger assays, τ also incorporates the receptor number, thus, values were corrected for relative surface expression (SI Fig. 1) to obtain τ_c . Errors of surface expression determination were propagated. Saturation BRET experiments for basal and agonist-stimulated states were fit for one site total binding to account for a nonspecific component by random collision (bystander BRET), and $BRET_{50}$ as well as max. BRET are reported.

RESULTS

Affinity of NPY binding is not affected by W6.48

Our recent model of NPY bound to the Y₂R (Kaiser *et al.*, 2015) has identified a hydrophobic patch in ECL2 guiding the binding path of the peptide through its amphipathic helix (Fig. 1), and explained the significance of several previously known mutations of peptide and receptor for binding. Most interestingly, we were able to characterize a deep transmembrane binding pocket for the C-terminus of the peptide. Central to this pocket are contacts of the C-terminal peptide amide and the side chain of Q³⁴ to Q^{3.32} in TM3 of the receptor. The positioning of Y³⁶ in a long but narrow binding pocket between TM3, TM6, and TM7 was furthermore found. This brings Y³⁶ in a T-shaped configuration relative to W^{6.48}, a highly conserved residue within rhodopsin-like GPCRs that has been suggested to be part of a toggle switch (Schwartz *et al.*, 2006; Holst *et al.*, 2010). The side chain conformation of W^{6.48} in the Y₂R model was fixed to the available crystallographic data (Katritch *et al.*, 2013), which all displayed a very similar orientation with the imidazole ring roughly perpendicular to the membrane plane (Fig. 1). Depending on the exact positioning, this would allow for binding contributions of W^{6.48} by T-shaped π - π -interactions and/or a 'domino-effect' in which the side chain of Y³⁶ slightly displaces W^{6.48}, and thus potentially initiates receptor activation as for instance suggested from comparison of rhodopsin structures in different activity states (Scheerer *et al.*, 2008) and MD simulations of adenosine A_{2A} receptor (Li *et al.*, 2013). To define the role of W^{6.48} for Y₂R ligand binding and activation, we mutated this residue and first tested binding affinities.

To our surprise, a conservative mutation of W^{6.48} to phenylalanine was not tolerated, and caused defective folding and retention in intracellular compartments, most likely in the endoplasmic reticulum as demonstrated by microscopy of eYFP-fusion proteins (Supplemental Figure 1). While purely hydrophobic exchanges to leucine, isoleucine or alanine were also folding deficient, exchange to tyrosine, histidine and also the small, non-aromatic threonine was accepted (Fig. S1), and investigated in more detail.

We performed saturation binding experiments of ^{125}I -PYY at membrane preparations of transiently transfected HEK293-cells. These experiments demonstrated wild type like affinities of c. 50 pM for all variants and only a moderate loss of receptor expression level (B_{max} $W^{6.48}\text{Y}$ 60% of WT, $W^{6.48}\text{H}$ 65%, $W^{6.48}\text{T}$ 79%; Fig. 2A and Tab. 1). In addition, displacement binding experiments with NPY confirmed unchanged affinities compared to wild type receptor (Fig. 2B). Remarkably, half-maximal displacement (IC_{50}) occurred in the 2-3 nM range, equivalent to K_i values of the NPY competitor of ~1 nM. Since displacement of ^{125}I -PYY with NPY is quasi-homologous, K_i (NPY) should match K_d (^{125}I -PYY) within experimental error. Alternatively, the two assay setups may reflect two different affinity states. We probed this hypothesis by recording the kinetics of radioligand dissociation as shown in Figure 2C. Indeed, radioligand dissociation clearly followed a two-phase behavior with a ratio of the two time constants ($k_{\text{slow}}/k_{\text{fast}}$) of ~50 for all variants ($k_{\text{off,slow}} = 0.007 \text{ min}^{-1}$; $k_{\text{off,fast}} = 0.41 \text{ min}^{-1}$ for WT Y_2R). Taking into account the association rate constant, which we determined to $k_{\text{on}} = 6.4 \times 10^{-4} \text{ pM}^{-1} \text{ min}^{-1}$ (Fig. 2D), this yields a kinetic K_d of 11 pM and 641 pM for the high and low affinity state of the wild type receptor, respectively, matching the observed affinity differences reasonably well. Moreover, close examination of the displacement experiments reveals some deviation of the curves from the standard steepness, and curves may be approximated better by assuming two affinity states at ~0.5 nM and ~11 nM (Fig. 2C). We speculated that the high-affinity state might be stabilized by G_i -binding, and thus repeated dissociation experiments in the presence of 100 μM $\text{GTP}\gamma\text{S}$, a non-hydrolyzable GTP analogue that should disrupt the high affinity Y_2R - G_i complex (no nucleotide bound). Indeed, the presence of $\text{GTP}\gamma\text{S}$ shifted the kinetics towards the fast phase representing the low-affinity state for the wild type Y_2 receptor as well as all $W^{6.48}$ variants (Fig. 2C,D). Hence, mutagenesis of $W^{6.48}$ did not affect the affinity of the receptor for its ligand NPY, neither for the high affinity state supposedly stabilized by G protein nor the lower-affinity state.

$W^{6.48}$ is critical to activate downstream effectors

Next, we were interested in how signal transduction of the receptor might be changed by mutation of $W^{6.48}$. We first measured the ability of the mutated receptors to elicit the accumulation of a second messenger by using a well-established chimeric G protein ($G_{\alpha_{\Delta 6qi4myr}}$) redirecting the native G_i signaling to the phospholipase C pathway (Kostenis *et al.*, 2005), which has also been applied in previous structure-activity and complementary mutagenesis studies (Merten *et al.*, 2007; Kaiser *et al.*, 2015), and allows for robust readout with superb signal-to-noise ratio. Mutation of $W^{6.48}$ mainly led to a shift in potency, with 5-10 fold right-shifted EC_{50} in the order $Y < T = H$, and only slightly reduced E_{max} (Fig. 3A). Next, the data were analyzed using the operational model of agonism (Black and Leff, 1983). For concentration-response-curves with significant reduction of E_{max} compared to the control curve, this analysis provides information about the transducer constant (efficacy term) τ and functional affinity K_A . However, any response that reaches close enough to the defined maximum response can be fit by some combinations of τ and K_A (Kenakin *et al.*, 2011; Kenakin and Christopoulos, 2013). Results may then depend on the individual errors of each data point and should therefore be taken with caution. Thus, the so-called “transduction coefficient term” τ/K_A was suggested as more robust measure of activity (Kenakin *et al.*, 2011; Kenakin and Christopoulos, 2013) for any shape of the concentration-response curve which, however, leads to the loss of direct information on the proportion to which a decreased activity is split into its τ and K_A components.

As expected, analysis of the IP accumulation of Y_2R and its $W^{6.48}$ mutants using the operational model resulted in significantly reduced transduction coefficients $\log \tau_c/K_A$ (corrected for surface expression). Due to the excellent signal-to-noise ratio and reproducibility of the assay, the analysis also allowed for some insight into K_A and efficacy term τ : While the functional affinity remained largely unaltered, τ and also its surface-expression corrected equivalent τ_c (see experimental section for details) were strongly reduced in the order $Y < T = H$ (Tab. 2), supportive of a role for $W^{6.48}$ in the activation of the Y_2R . In an analogous manner, we analyzed effects on the native G_i pathway using a CRE-reporter gene assay. Again, mutation of $W^{6.48}$

mainly shifted EC_{50} (Fig. 3B) in the order $Y < T \leq H$, which translated to reduced τ_c and transduction coefficients $\log(\tau_c/K_A)$ (Tab. 2).

A third relevant effector for the Y_2R is arrestin3 (Berglund *et al.*, 2003; Kilpatrick *et al.*, 2010; Walther *et al.*, 2010), which is generally suggested to mediate receptor desensitization, and might scaffold further signaling components such as MAP kinases (Lu *et al.*, 2010). Arrestin3 is only recruited to the Y_2R at relatively high agonist concentrations (Kilpatrick *et al.*, 2010), and contributes to receptor internalization (Walther *et al.*, 2010; Lundell *et al.*, 2011). We probed arrestin-recruitment by live cell fluorescence microscopy in cells co-transfected with mCherry-arrestin3 and Y_2R -eYFP fusion proteins (Fig. 4A). After stimulation with 1 μ M NPY, arrestin3 was robustly relocated from the cytoplasm to the cell membrane for at least 30 min. The $W^{6.48Y}$ variant also clearly recruited arrestin3 after ligand stimulation. This effect, however, appeared more transient as arrestin3 was distributed again in the cytoplasm after 30 min of agonist exposure. Remarkably, $W^{6.48H}$ and $W^{6.48T}$ showed a much weaker arrestin3 recruitment compared to the wild type Y_2R , albeit this weak arrestin3 recruitment was apparently stable for at least 30 min. Similar findings were also observed for the receptor internalization (Fig. 4B). While WT and $W^{6.48Y}$ were almost quantitatively internalized after 30 min of agonist stimulation, a large portion of the $W^{6.48H}$ and $W^{6.48T}$ variants was still present at the cell membrane even after 60 min of agonist exposure at 1 μ M concentration. These results strongly indicate that $W^{6.48}$ tunes signal transduction of the Y_2R for G protein and arrestin3 pathways. Interestingly, the effects on arrestin3 recruitment revealed differences between $W^{6.48Y}$ and $W^{6.48H/T}$.

BRET illuminates differential coupling of the Y_2R to its effectors

To be able to investigate the effects of $W^{6.48}$ mutagenesis on signal transduction in a more detailed and quantitative manner, BRET-sensors (bioluminescence resonance energy transfer) were constructed for chimeric $G_{\alpha_{\Delta 6qi4myr}}$, native G_{α_i} as well as arrestin3. This provides a system without amplification steps and thus identical assay sensitivity, which facilitates quantitative considerations. In addition to classic ligand concentration-response-curves, BRET

sensors can also provide information on receptor-effector affinities including pre-assembly phenomena, and easily give access to kinetic profiles of interaction. We inserted a monomeric variant (A²⁰⁶K) (Zacharias *et al.*, 2002) of the Venus-fluorophore into the helical domain of the G α -subunit as BRET acceptor to be used with C-terminal Y₂R-Rluc8 fusions (Gimenez *et al.*, 2014; Mäde *et al.*, 2014) as BRET donors. Functionality of the tagged G proteins was verified by IP accumulation assays (Supplemental Figure 2) and correct expression in the plasma membrane (Fig.5F). As specificity control, we used G $\alpha_{\Delta 6qmyr}$ bearing the natural G α_q C-terminal four amino acids, but truncated N-terminus similar to the chimeric G $\alpha_{\Delta 6qi4myr}$ (Fig. 5E,F). For arrestin3, we followed the established strategy with an N-terminal sensor (Vishnivetskiy *et al.*, 2011), but chose Rluc8 instead of Venus for a greater assay flexibility and an improved signal window.

We first performed saturation BRET-experiments between the receptor and G α_{i1} . As shown in Fig. 5A, there was significant and saturable BRET between all receptor variants and G α_{i1} even in the absence of ligand. The BRET signal was further increased by the addition of NPY. This strongly indicated pre-assembly of the complex. In fact, nonlinear regression revealed identical or even slightly higher BRET₅₀ pseudo-affinity constants, i.e. acceptor to donor ratio (F/L) yielding half-maximal BRET, for the receptor-G-protein-complex in the presence of ligand (Tab. 3). Such a result is commonly attributed to the conformational change of a complex rather than protein recruitment/binding, which would lead to an improved (=decreased) BRET₅₀ (Issad and Jockers, 2006). Pre-assembly is also corroborated by the kinetic profile of the BRET signals. The ligand-dependent increase of the BRET signal appeared to occur instantly, such that its initial kinetics could not be followed with our instrumentation (30 s lag between stimulation and first reading), and then remained stable for at least 15 min. Remarkably, none of the W^{6.48} mutations significantly affected pre-assembly or reduced the maximal ligand-dependent netBRET (Fig. 5A, bars), thus, the mutants were still able to fully activate the G_i pathway at 1 μ M NPY. However, ligand-concentration-response curves to evoke netBRET were right-shifted in the order W^{6.48}Y < T \leq H (Fig. 5B), confirming a weakened propagation of agonist-induced activation.

We observed similar trends also for the chimeric $G_{\alpha_{\Delta 6qi4myr}}$. In the absence of ligand, the chimeric G protein showed saturable binding to wild type Y_2R and the $W^{6.48}$ variants (Fig. 5C), and stimulation with NPY increased the BRET signal with apparently instant kinetics. Interestingly, despite exhibiting comparable $BRET_{50}$ values to $G_{\alpha_{i1}}$, the extent of basal interaction was reduced for $G_{\alpha_{\Delta 6qi4myr}}$ (max. basal BRET 0.08 vs 0.19 for WT Y_2R - $G_{\alpha_{\Delta 6qi4myr}}$ and $G_{\alpha_{i1}}$, respectively). Such a difference was not present for the maximal ligand-induced netBRET (0.04 vs 0.05), indicating a different initial conformation of the chimeric G protein, which becomes aligned during G protein activation (Tab. 3). In addition, ligand stimulation went along with improved $BRET_{50}$ between Y_2R and $G_{\alpha_{\Delta 6qi4myr}}$ (Tab. 3), corroborating differences in the interaction. Ligand-induced $G_{\alpha_{\Delta 6qi4myr}}$ activation was significantly affected by the mutation of $W^{6.48}$. The netBRET in response to 1 μM NPY was reduced for all variants while the amount of pre-assembly remained comparable (Fig. 5C). This can be followed in more detail in ligand concentration-response curves recorded at saturating F/L ratio (Fig. 5D), which were right-shifted in the order $W^{6.48}Y < T < H$. As judged from the EC_{50} values, $G_{\alpha_{\Delta 6qi4myr}}$ is about 10-fold less efficiently activated than $G_{\alpha_{i1}}$ by wild type Y_2R and the native ligand NPY. Accordingly, $W^{6.48}$ mutants shifted even further and were only fully activated at 10 μM NPY, with the exception of $W^{6.48}H$, where saturation could not be reached even at this very high concentration.

Next, we probed arrestin3 recruitment by BRET. As expected from the microscopy data, arrestin3 was only recruited to the receptor in the presence of ligand (1 μM) and no basal interaction was observed (Fig. 6A). The recruitment was slow and reached a stable plateau 10 min after stimulation with NPY for the wild type, $W^{6.48}H$ and $W^{6.48}T$ Y_2R . Interestingly, the $W^{6.48}Y$ variant displayed more transient kinetics with maximum signal after 5 min which quickly declined again (Fig. 6C). At their respective signal maxima after 10 min and 5 min of stimulation, respectively, the $W^{6.48}$ mutants displayed significantly impaired arrestin3 recruitment with more than 50% decreased netBRET after NPY stimulation, with the $W^{6.48}H$ variant again being most deleterious. Notably, the BRET ratio (and thus possible maximum

netBRET) is independent of the receptor expression level as long as measurements are performed at saturating F/L ratio, (Terrillon *et al.*, 2003; Borroto-Escuela *et al.*, 2013), which was assured ($F/L > 0.012$, i.e. $\geq 3x$ BRET₅₀ for any construct). Accordingly, netBRET reductions indicate that the active-state cannot be fully populated. This was also reflected in ligand-concentration response curves recorded at saturating F/L ratios (Fig. 6B). All W^{6.48} mutants displayed a reduced E_{max}/netBRET, but differed in their EC₅₀ values. While W^{6.48}Y displayed an identical EC₅₀ like WT Y₂R (WT: 76 nM, W^{6.48}Y: 84 nM), W^{6.48}T (EC₅₀: 368 nM) and W^{6.48}H (EC₅₀: 970 nM) required significantly higher ligand concentrations for maximal arrestin3 recruitment.

Designed ligands can restore arrestin3-recruitment

We speculated that the impaired signal transduction of the W^{6.48} variants is likely caused by a sterical component, i.e. the large tryptophan side chain might contribute to the opening of the intracellular effector binding site. Thus, we aimed to compensate the effects of W^{6.48} mutation by using NPY ligands with modifications at position 36. To this end, we synthesized naphthylalanine (Nal)³⁶-NPY peptide analogues, which have previously been described to remain active in a G_i second messenger readout at wild type Y₂R (Albertsen *et al.*, 2013). Two different configurations are possible, 1Nal resembles the indole ring conjunction of tryptophan (ortho-meta-substitution at the phenylring), while 2Nal is extended at the meta-para position (Fig. 7). We tested both peptides for receptor binding, activation of G_{α₁} and chimeric G_{α_{Δ6qi4myr}}, and probed arrestin3 recruitment.

Despite its size, 2Nal³⁶-NPY is accepted very well in the binding pocket and displayed only a very mild decrease in affinity at the wild type Y₂R and all W^{6.48} variants (Tab. 5), underlining the notion of a long binding pocket between TM2 and TM7 (Kaiser *et al.*, 2015). Interestingly, the wider conformation of 1Nal³⁶-NPY distinguished between the W^{6.48} mutants. 1Nal³⁶-NPY did not affect the binding affinity to the wild type Y₂R (IC₅₀ WT Y₂R-NPY: 2.6 nM, 1Nal³⁶: 3.9 nM) or W^{6.48}Y, but showed significantly increased affinity to W^{6.48}H and W^{6.48}T variants (IC₅₀ W^{6.48}H: 0.4 nM, W^{6.48}T: 0.6 nM). Since this increase in affinity was similar for the variants with

an aromatic histidine and small threonine side chain at position 6.48, and not present for the wild type tryptophan, it is likely not caused by π -interactions of the naphthyl-substituent to position 6.48. Rather, $W^{6.48}H/T$ mutation might constrict or twist the binding pocket such that the $1NaI^{36}$ substituent, but not the $2NaI^{36}$ counterpart, is placed optimally and creates an increased affinity over the wild type binding pocket.

Indeed, $1NaI^{36}$ -NPY and $2NaI^{36}$ -NPY also affected signaling differently. Very much in analogy to the minimally decreased binding affinity, the $2NaI^{36}$ -NPY induced activation of $G_{\alpha_{i1}}$ was shifted by a factor of two at the wild type Y_2R and all $W^{6.48}$ mutants, which similarly also holds for the activation of chimeric $G_{\alpha_{\Delta 6qj4myr}}$ and recruitment of arrestin3 (Fig. 7, bottom row). In contrast, stimulation with $1NaI^{36}$ -NPY did not affect signaling of the wild type Y_2R and the $W^{6.48}Y$ variant, but was able to restore signaling of the $W^{6.48}H$ and $W^{6.48}T$ variants back to wild type levels. Most strikingly, not only the affinity/potency was rescued for G protein pathways, but also the efficiency of arrestin3 recruitment could be significantly increased (netBRET(95%CI) $W^{6.48}H$ -NPY: 0.25 (0.23-0.28), $W^{6.48}H$ - $1NaI^{36}$: 0.36 (0.33-0.39); Fig. 7, middle row). This clearly underlines that a correctly placed bulky lever is required for efficient recruitment of arrestin3 at the Y_2R , and the $1NaI^{36}$ -substituent can take over this function from the endogenous $W^{6.48}$.

DISCUSSION

Several crystallographic structures have suggested a common binding crevice within the transmembrane core of GPCRs of up to 14 Å in depth (Venkatakrisnan *et al.*, 2013). In many instances, this also involves W^{6.48} (Venkatakrisnan *et al.*, 2013), suggesting that ligand contacts directly modulate the ‘transmission switch’ that consists of a cluster of hydrophobic residues (3.40, 5.51, 6.44 and 6.48) (Deupi and Standfuss, 2011; Venkatakrisnan *et al.*, 2013; Tehan *et al.*, 2014). Such a deep binding site is also partly seen in co-crystals involving peptide ligands (Venkatakrisnan *et al.*, 2013; Krumm and Grisshammer, 2015) although this might not *a priori* be expected. Recently, we presented a model of a 24-amino acid truncated NPY variant (NPY¹³⁻³⁶) bound to the Y₂R (Kaiser *et al.*, 2015), which also displayed a deep binding mode that reaches down to W^{6.48}, and we were interested in how this residue modulates binding and activation of the receptor.

Based on our data, we present the following model of effector coupling to the Y₂R (Fig. 8): The Y₂R displays equal affinities to the inactive G_i(GDP)-heterotrimer in the basal (R) and activated state (LR*), and forms pre-assembled complexes already in the absence of ligand. Ligand binding causes W^{6.48} to relocate and catalyzes GDP release accompanied by structural rearrangement of the complex (Alexander *et al.*, 2013; Hamm *et al.*, 2013), enabling GTP binding and activation of the G_i pathway. Arrestin3 recruitment, in contrast, only occurs after receptor activation in agreement with the accepted models and is critically dependent on the opening of the intracellular crevice by the bulky side chain of W^{6.48}. Mutation of this amino acid weakens the allosteric coupling between the ligand and effector binding sites, which attenuates arrestin recruitment. Pre-assembly of G_i to the receptor, however, is very robust and not affected by such mutations, implying that the intracellular crevice is still wide enough to accommodate the C-terminal α5-helix of Gα_i. We suggest that this pre-assembly and ‘readiness’ of the G protein ensures full activation of the pathway (E_{max}) despite the weakened allosteric coupling in W^{6.48} mutants. In this case, the lack of stabilization of the active state requires more frequent ligand binding events (higher receptor occupancy) to catalyze GDP release, which is reflected in apparently reduced ligand potencies to G_i.

Binding characteristics of the Y₂R

Notably, W^{6.48} functioned as allosteric connector for receptor activation, but did not significantly contribute to ligand affinity. Investigation of the binding properties of wild type and mutant Y₂R moreover revealed two affinity states. Ligand binding to the activated R*-G-protein complex (nucleotide free) displayed a very high affinity with picomolar dissociation constant, and was confirmed by the sensitivity to GTP γ S treatment (Fig. 2C). Ligand binding to the receptor alone or with pre-assembled G-protein (GDP-bound), however, displayed a moderate affinity of about 1 nM, and represents the relevant state for ligand-induced activation of the receptor in the biological context. The recognition of two affinity sites might also bring together apparently contradictory findings on Y₂R K_D values in the past using ³H-radioligands (0.5-0.7 nM) (Höfliger *et al.*, 2003; Ziemek *et al.*, 2006), and the more sensitive ¹²⁵I-radionuclides (K_D around 20 pM) (Salaneck *et al.*, 2000; Xu *et al.*, 2013), respectively, and rationalize discrepancies reported between K_D and K_i in homologous displacement experiments (Xu *et al.*, 2013), very much in analogy to our results.

Intriguingly, the strong positive cooperativity of ligand binding and G protein activation for the Y₂R also leads to some deviation from the proposed allosteric mechanism linking ligand and effector binding pockets (Freissmuth *et al.*, 1991; DeVree *et al.*, 2016). For the β_2 AR and selected other GPCRs, bound G protein or nanobody reduces the total ligand binding to the complex by occlusion of the binding pocket. Conversely, uncoupling of the complex by the addition of GTP γ S increases k_{on} at these receptors, which allows for a greater maximal ligand binding (Freissmuth *et al.*, 1991; DeVree *et al.*, 2016). For the Y₂R, however, we (Fig. 2C) and others (Freitag *et al.*, 1995) observed strongly decreased total agonist binding in the uncoupled state (+GTP γ S). We attribute this to insufficient ligand affinity in the absence of G protein. However, we found slowed k_{off} of the radioligand from the Y₂R-G protein complex similar to other GPCRs (DeVree *et al.*, 2016) supporting the concept of a stabilized agonist binding pocket in the GPCR-effector-complex.

Steric and polar requirements at position 6.48 for activation of the Y₂R

By analyzing different W^{6.48} mutants and complementary ligands, we were able to gain more insight into the molecular mechanism of activation. The role of W^{6.48} for the communication of ligand binding contains a steric component as the effects of smaller amino acids at this position (W^{6.48}T/W^{6.48}H) could largely be compensated by ligands carrying a bulky 1Nal-substituent at the C-terminal ligand position. The specificity of this effect was underlined by the lack of a similar rescuing effect for a 2Nal substituent. Of note, stimulation with 1Nal³⁶-NPY did not only restore the ligand potency for the activation of G_i and chimeric G $\alpha_{\Delta 6\text{qi}4\text{myr}}$, but also increased the maximal netBRET of arrestin3 recruitment almost back to wild type level for the W^{6.48}H and W^{6.48}T variants (Fig. 7, Tab. 5). This implies re-enforcement of the allosteric connection, which restores the conformational coupling between the receptor and the $\alpha 5$ -helix of G_i, and leads to a wider opening of the intracellular crevice, thus regaining the ability to bind the arrestin fingerloop (referred to as 'core-conformation' (Shukla *et al.*, 2014)).

Our data also provide support for contributions of a specific polar interaction network involved in the regulation of Y₂R activation as suggested for other receptors (Valentin-Hansen *et al.*, 2015; Yuan *et al.*, 2015): (i) Unpolar amino acids were not accepted and led to misfolded receptors that were retained in the ER. Thus, hydrogen bonding capacities seem to be highly conserved and vital for Y₂R function. (ii) Mutation of W^{6.48} to the relatively large, aromatic histidine was more deleterious compared to the small threonine. Most likely, these alterations arise from altered hydrogen bonding in the core of the receptor due to a different positioning of the hydrogen bond donor (NH/OH) compared to the original indole side chain of tryptophan.

Y₂R displays a strong inherent bias for G_i over arrestin3 which is maintained in W^{6.48} mutants

The pre-assembly of G_i to the Y₂R appeared very robust even after mutagenesis of W^{6.48}, and is an important hallmark of Y₂R-effector interactions. Interestingly, similar data have been obtained by *in vitro* (Alves *et al.*, 2003, 2005) as well as BRET studies (Galés *et al.*, 2006; Audet *et al.*, 2008) of other G_i-coupled GPCRs, suggesting this to emerge as a more common mechanism at least for this class of G proteins that might be facilitated by the slim shape of

G_{α_i} C-terminus (Rose *et al.*, 2014). To evaluate whether pre-assembly is also reflected in signaling balance, we quantitatively compared the responses of wild type and mutant receptors to different pathways. The wild type receptor inherently activated G_i about 1.24 orders of magnitude more efficiently than it recruited arrestin ($\log(\tau/K_A)$ for $G_i = 8.39$; $\text{arr3} = 7.15$, Tab. 5). Interestingly, activation of the chimeric G_{iq} was also significantly less efficient ($\log(\tau/K_A)$ for $G_{iq} = 7.33$) compared to the native G_i , underlining differences in the receptor interaction. Of note, pre-assembly did not *per se* reduce requirements for G_i (or G_{iq}) activation: Comparison of transduction coefficients $\Delta\log(\tau/K_A)$ between WT and mutant for a given pathway demonstrates that mutagenesis of $W^{6.48}$ generally resulted in a similar loss of function for G_i versus arrestin3 interaction (Tab. 5), i.e. mutation of $W^{6.48}$ did not induce signaling bias.

Thus, in general terms, $W^{6.48}$ controlled the activation of downstream effectors in a similar manner and did not contribute significantly to the preference for G_i activation over arrestin3 recruitment. Similarly, introduction of sterically demanding side chains at the C-terminal residue of the peptide did not shift signaling of WT Y_2R to the benefit of arrestin3. Thus, alternative positions should be considered if aiming at the design of arrestin3-preferring ligands at this receptor. Given the highly robust interaction of the Y_2R with inhibitory G proteins and the similar requirements for activation/recruitment, however, design of such ligands might prove difficult.

Conclusions

The present study demonstrates $W^{6.48}$ to function as an allosteric connector between the ligand binding pocket and effector activation at the neuropeptide Y_2R . In agreement with our model of NPY-bound Y_2R (Kaiser *et al.*, 2015), we confirmed that the C-terminus of the peptide reaches deeply into the transmembrane core of the receptor, and modulates the conformation of $W^{6.48}$. In contrast to previous studies at other GPCRs (Holst *et al.*, 2010; Krumm *et al.*, 2015; Valentin-Hansen *et al.*, 2015), mutagenesis of $W^{6.48}$ did not result in a complete loss of signaling. We suggest that a combination of deep binding mode and G_i pre-assembly rescues full activation of the G_i pathway at high ligand concentrations. In contrast, arrestin3 recruitment

requires opening of the intracellular crevice to a greater extent, and mutation of W^{6.48} goes along with reduced receptor-arrestin complex formation.

ACKNOWLEDGMENTS

The authors would like to thank R. Steinborn for help with cloning and initial characterization of tagged chimeric G proteins, and C.Hartig for cloning of the Gq Δ 6-Venus protein. We gratefully acknowledge the skilled technical assistance of C. Dammann, K. Löbner, R.Reppich-Sacher and J. Schwesinger.

AUTHORSHIP CONTRIBUTIONS

Participated in research design: Kaiser, Beck-Sickinger

Conducted experiments: Kaiser, Hempel, Wanka, Schubert

Contributed new reagents or analytic tools: n.a.

Performed data analysis: Kaiser, Hempel, Wanka, Schubert, Hamm, Beck-Sickinger

Wrote or contributed to the writing of the manuscript: Kaiser, Hamm, Beck-Sickinger

REFERENCES

- Albertsen L, Østergaard S, Paulsson JF, Norrild JC, and Strømgaard K (2013) A parallel semisynthetic approach for structure-activity relationship studies of peptide YY. *ChemMedChem* **8**:1505–1513, 1422.
- Alexander NS, Preininger AM, Kaya AI, Stein RA, Hamm HE, and Meiler J (2013) Energetic analysis of the rhodopsin–G-protein complex links the $\alpha 5$ helix to GDP release. *Nat Struct Mol Biol* **21**:56–63.
- Alves ID, Salamon Z, Varga E, Yamamura HI, Tollin G, and Hruby VJ (2003) Direct Observation of G-protein Binding to the Human μ -Opioid Receptor Using Plasmon-Waveguide Resonance Spectroscopy. *J Biol Chem* **278**:48890–48897.
- Alves ID, Salgado GFJ, Salamon Z, Brown MF, Tollin G, and Hruby VJ (2005) Phosphatidylethanolamine Enhances Rhodopsin Photoactivation and Transducin Binding in a Solid Supported Lipid Bilayer as Determined Using Plasmon-Waveguide Resonance Spectroscopy. *Biophys J* **88**:198–210.
- Audet N, Gales C, Archer-Lahlou E, Vallieres M, Schiller PW, Bouvier M, and Pineyro G (2008) Bioluminescence Resonance Energy Transfer Assays Reveal Ligand-specific Conformational Changes within Preformed Signaling Complexes Containing μ -Opioid Receptors and Heterotrimeric G Proteins. *J Biol Chem* **283**:15078–15088.
- Babilon S, Mörl K, and Beck-Sickinger AG (2013) Towards improved receptor targeting: anterograde transport, internalization and postendocytic trafficking of neuropeptide Y receptors. *Biol Chem* **394**:921–936.
- Ballesteros JA, and Weinstein H (1995) Integrated methods for the construction of three-dimensional models and computational probing of structure-function relations in G protein-coupled receptors, in *Methods in Neurosciences* (Stuart C. Sealson ed) pp 366–428, Academic Press.
- Beck-Sickinger AG, Wieland HA, Wittneben H, Willim KD, Rudolf K, and Jung G (1994) Complete L-alanine scan of neuropeptide Y reveals ligands binding to Y1 and Y2 receptors with distinguished conformations. *Eur J Biochem FEBS* **225**:947–958.
- Berglund MM, Schober DA, Statnick MA, McDonald PH, and Gehlert DR (2003) The use of bioluminescence resonance energy transfer 2 to study neuropeptide Y receptor agonist-induced beta-arrestin 2 interaction. *J Pharmacol Exp Ther* **306**:147–156.
- Black J, and Leff P (1983) Operational Models of Pharmacological Agonism. *Proc R Soc Lond B Biol Sci* **220**:141–62.
- Borroto-Escuela DO, Flajolet M, Agnati LF, Greengard P, and Fuxe K (2013) Bioluminescence resonance energy transfer methods to study G protein-coupled receptor-receptor tyrosine kinase heteroreceptor complexes. *Methods Cell Biol* **117**:141–164.
- Deupi X, and Standfuss J (2011) Structural insights into agonist-induced activation of G-protein-coupled receptors. *Curr Opin Struct Biol* **21**:541–551.
- DeVree BT, Mahoney JP, Vélez-Ruiz GA, Rasmussen SGF, Kuszak AJ, Edwald E, Fung J-J, Manglik A, Masureel M, Du Y, Matt RA, Pardon E, Steyaert J, Kobilka BK, and Sunahara RK (2016) Allosteric coupling from G protein to the agonist-binding pocket in GPCRs. *Nature* **535**:182–186.

- Dinger MC, Bader JE, Kobor AD, Kretschmar AK, and Beck-Sickinger AG (2003) Homodimerization of neuropeptide γ receptors investigated by fluorescence resonance energy transfer in living cells. *J Biol Chem* **278**:10562–10571.
- Egloff P, Hillenbrand M, Klenk C, Batyuk A, Heine P, Balada S, Schlinkmann KM, Scott DJ, Schutz M, and Pluckthun A (2014) Structure of signaling-competent neurotensin receptor 1 obtained by directed evolution in *Escherichia coli*. *Proc Natl Acad Sci* **111**:E655–E662.
- Els S, Beck-Sickinger AG, and Chollet C (2010) Ghrelin receptor: high constitutive activity and methods for developing inverse agonists. *Methods Enzymol* **485**:103–121.
- Freissmuth M, Selzer E, and Schütz W (1991) Interactions of purified bovine brain A1-adenosine receptors with G-proteins. Reciprocal modulation of agonist and antagonist binding. *Biochem J* **275**:651–656.
- Freitag C, Svendsen AB, Feldthus N, Løssl K, and Sheikh SP (1995) Coupling of the human Y2 receptor for neuropeptide Y and peptide YY to guanine nucleotide inhibitory proteins in permeabilized SMS-KAN cells. *J Neurochem* **64**:643–650.
- Galés C, Van Durm JJJ, Schaak S, Pontier S, Percherancier Y, Audet M, Paris H, and Bouvier M (2006) Probing the activation-promoted structural rearrangements in preassembled receptor–G protein complexes. *Nat Struct Mol Biol* **13**:778–786.
- Garland SL (2013) Are GPCRs still a source of new targets? *J Biomol Screen* **18**:947–966.
- Gimenez LE, Babilon S, Wanka L, Beck-Sickinger AG, and Gurevich VV (2014) Mutations in arrestin-3 differentially affect binding to neuropeptide Y receptor subtypes. *Cell Signal* **26**:1523–1531.
- Hamm HE, Kaya AI, Gilbert JA, and Preininger AM (2013) Linking receptor activation to changes in Sw I and II of G α proteins. *J Struct Biol* **184**:63–74.
- Höfliger MM, Castejón GL, Kiess W, and Beck Sickinger AG (2003) Novel cell line selectively expressing neuropeptide Y-Y2 receptors. *J Recept Signal Transduct Res* **23**:351–360.
- Holst B, Nygaard R, Valentin-Hansen L, Bach A, Engelstoft MS, Petersen PS, Frimurer TM, and Schwartz TW (2010) A conserved aromatic lock for the tryptophan rotameric switch in TM-VI of seven-transmembrane receptors. *J Biol Chem* **285**:3973–3985.
- Hopkins AL, and Groom CR (2002) The druggable genome. *Nat Rev Drug Discov* **1**:727–730.
- Issad T, and Jockers R (2006) Bioluminescence resonance energy transfer to monitor protein-protein interactions. *Methods Mol Biol* **332**:195–209.
- Kaiser A, Müller P, Zellmann T, Scheidt HA, Thomas L, Bosse M, Meier R, Meiler J, Huster D, Beck-Sickinger AG, and Schmidt P (2015) Unwinding of the C-Terminal Residues of Neuropeptide Y is critical for Y2 Receptor Binding and Activation. *Angew Chem Int Ed Engl* **54**:7446–7449.
- Katritch V, Cherezov V, and Stevens RC (2013) Structure-function of the G protein-coupled receptor superfamily. *Annu Rev Pharmacol Toxicol* **53**:531–556.
- Kenakin T, and Christopoulos A (2013) Signalling bias in new drug discovery: detection, quantification and therapeutic impact. *Nat Rev Drug Discov* **12**:205.

- Kenakin T, Watson C, Muniz-Medina V, Christopoulos A, and Novick S (2011) A Simple Method for Quantifying Functional Selectivity and Agonist Bias. *ACS Chem Neurosci* **3**:193–203.
- Khoury E, Clément S, and Laporte SA (2014) Allosteric and biased g protein-coupled receptor signaling regulation: potentials for new therapeutics. *Front Endocrinol* **5**:68.
- Kilpatrick L, Briddon SJ, Hill SJ, and Holliday ND (2010) Quantitative analysis of neuropeptide Y receptor association with β -arrestin2 measured by bimolecular fluorescence complementation - Kilpatrick - 2010 - British Journal of Pharmacology - Wiley Online Library. *Br J Pharmacol* **160**:892–906.
- Kostenis E, Waelbroeck M, and Milligan G (2005) Techniques: promiscuous Galpha proteins in basic research and drug discovery. *Trends Pharmacol Sci* **26**:595–602.
- Krumm BE, and Grisshammer R (2015) Peptide ligand recognition by G protein-coupled receptors. *Front Pharmacol* **6**.
- Krumm BE, Lee S, Bhattacharya S, Botos I, White CF, Du H, Vaidehi N, and Grisshammer R (2016) Structure and dynamics of a constitutively active neurotensin receptor. *Sci Rep* **6**:38564.
- Krumm BE, White JF, Shah P, and Grisshammer R (2015) Structural prerequisites for G-protein activation by the neurotensin receptor. *Nat Commun* **6**:7895.
- Li J, Jonsson AL, Beuming T, Shelley JC, and Voth GA (2013) Ligand-dependent activation and deactivation of the human adenosine A(2A) receptor. *J Am Chem Soc* **135**:8749–8759.
- Loening AM, Fenn TD, Wu AM, and Gambhir SS (2006) Consensus guided mutagenesis of Renilla luciferase yields enhanced stability and light output. *Protein Eng Des Sel PEDS* **19**:391–400.
- Lu C, Everhart L, Tilan J, Kuo L, Sun C-CJ, Munivenkatappa RB, Jönsson-Rylander A-C, Sun J, Kuan-Celarié A, Li L, Abe K, Zukowska Z, Toretsky JA, and Kitlinska J (2010) Neuropeptide Y and its Y2 receptor: potential targets in neuroblastoma therapy. *Oncogene* **29**:5630–5642.
- Lundell I, Rabe Bernhardt N, Johansson AK, and Larhammar D (2011) Internalization studies of chimeric neuropeptide Y receptors Y1 and Y2 suggest complex interactions between cytoplasmic domains. - PubMed - NCBI. *Regul Pept* **168**:50–58.
- Mäde V, Babilon S, Jolly N, Wanka L, Bellmann-Sickert K, Diaz Gimenez LE, Mörl K, Cox HM, Gurevich VV, and Beck-Sickinger AG (2014) Peptide modifications differentially alter g protein-coupled receptor internalization and signaling bias. *Angew Chem Int Ed Engl* **53**:10067–10071.
- Merten N, Lindner D, Rabe N, Römpler H, Mörl K, Schöneberg T, and Beck-Sickinger AG (2007) Receptor subtype-specific docking of Asp6.59 with C-terminal arginine residues in Y receptor ligands. *J Biol Chem* **282**:7543–7551.
- Michel MC, Beck-Sickinger A, Cox H, Doods HN, Herzog H, Larhammar D, Quirion R, Schwartz T, and Westfall T (1998) XVI. International Union of Pharmacology Recommendations for the Nomenclature of Neuropeptide Y, Peptide YY, and Pancreatic Polypeptide Receptors. *Pharmacol Rev* **50**:143–150.
- Nagai T, Ibata K, Park ES, Kubota M, Mikoshiba K, and Miyawaki A (2002) A variant of yellow fluorescent protein with fast and efficient maturation for cell-biological applications. *Nat Biotechnol* **20**:87–90.

- Oldham WM, and Hamm HE (2008) Heterotrimeric G protein activation by G-protein-coupled receptors. *Nat Rev Mol Cell Biol* **9**:60–71.
- Pedragosa-Badia X, Stichel J, and Beck-Sickinger AG (2013) Neuropeptide Y receptors: how to get subtype selectivity. *Front Endocrinol* **4**:5.
- Rajagopal S, Rajagopal K, and Lefkowitz RJ (2010) Teaching old receptors new tricks: biasing seven-transmembrane receptors. *Nat Rev Drug Discov* **9**:373–386.
- Rose AS, Elgeti M, Zachariae U, Grubmüller H, Hofmann KP, Scheerer P, and Hildebrand PW (2014) Position of transmembrane helix 6 determines receptor G protein coupling specificity. *J Am Chem Soc* **136**:11244–11247.
- Salaneck E, Holmberg SKS, Berglund MM, Boswell T, and Larhammar D (2000) Chicken neuropeptide Y receptor Y2: structural and pharmacological differences to mammalian Y2(1). *FEBS Lett* **484**:229–234.
- Scheerer P, Park JH, Hildebrand PW, Kim YJ, Krauss N, Choe H-W, Hofmann KP, and Ernst OP (2008) Crystal structure of opsin in its G-protein-interacting conformation. *Nature* **455**:497–502.
- Schwartz TW, Frimurer TM, Holst B, Rosenkilde MM, and Elling C (2006) Molecular Mechanism of 7TM Receptor Activation - A Global Toggle Switch Model. *Annu Rev Pharmacol Toxicol* **46**:481–519.
- Schwartz TW, and Rosenkilde MM (1996) Is there a “lock” for all agonist “keys” in 7TM receptors? *Trends Pharmacol Sci* **17**:213–216.
- Shukla AK, Westfield GH, Xiao K, Reis RI, Huang L-Y, Tripathi-Shukla P, Qian J, Li S, Blanc A, Oleskie AN, Dosey AM, Su M, Liang C-R, Gu L-L, Shan J-M, Chen X, Hanna R, Choi M, Yao XJ, Klink BU, Kahsai AW, Sidhu SS, Koide S, Penczek PA, Kossiakoff AA, Jr VLW, Kobilka BK, Skiniotis G, and Lefkowitz RJ (2014) Visualization of arrestin recruitment by a G-protein-coupled receptor. *Nature* **512**:218–222.
- Tehan BG, Bortolato A, Blaney FE, Weir MP, and Mason JS (2014) Unifying Family A GPCR Theories of Activation. *Pharmacol Ther* **143**:51–60.
- Terrillon S, Durroux T, Mouillac B, Breit A, Ayoub MA, Taulan M, Jockers R, Barberis C, and Bouvier M (2003) Oxytocin and vasopressin V1a and V2 receptors form constitutive homo- and heterodimers during biosynthesis. *Mol Endocrinol Baltim Md* **17**:677–691.
- Valentin-Hansen L, Frimurer TM, Mokrosinski J, Holliday ND, and Schwartz TW (2015) Biased Gs Versus Gq Proteins and β -Arrestin Signaling in the NK1 Receptor Determined by Interactions in the Water Hydrogen Bond Network. *J Biol Chem* **290**:24495–24508.
- Venkatakrishnan AJ, Deupi X, Lebon G, Tate CG, Schertler GF, and Babu MM (2013) Molecular signatures of G-protein-coupled receptors. *Nature* **494**:185–194.
- Vishnivetskiy SA, Gimenez LE, Francis DJ, Hanson SM, Hubbell WL, Klug CS, and Gurevich VV (2011) Few Residues within an Extensive Binding Interface Drive Receptor Interaction and Determine the Specificity of Arrestin Proteins. *J Biol Chem* **286**:24288–24299.
- Walther C, Nagel S, Gimenez LE, Mörl K, Gurevich VV, and Beck-Sickinger AG (2010) Ligand-induced internalization and recycling of the human neuropeptide Y2 receptor is regulated by its carboxyl-terminal tail. *J Biol Chem* **285**:41578–41590.

- White JF, Noinaj N, Shibata Y, Love J, Kloss B, Xu F, Gvozdenovic-Jeremic J, Shah P, Shiloach J, Tate CG, and Grisshammer R (2012) Structure of the agonist-bound neurotensin receptor. *Nature* **490**:508–513.
- Witte K, Kaiser A, Schmidt P, Splith V, Thomas L, Berndt S, Huster D, and Beck-Sickinger AG (2013) Oxidative in vitro folding of a cysteine deficient variant of the G protein-coupled neuropeptide Y receptor type 2 improves stability at high concentration. *Biol Chem* **394**:1045–1056.
- Wu F, Song G, de Graaf C, and Stevens RC (2017) Structure and Function of Peptide-Binding G Protein-Coupled Receptors. *J Mol Biol* **429**:2726–2745.
- Xu B, Fällmar H, Boukharta L, Pruner J, Lundell I, Mohell N, Gutiérrez-de-Terán H, Aqvist J, and Larhammar D (2013) Mutagenesis and computational modeling of human G-protein-coupled receptor Y2 for neuropeptide Y and peptide YY. *Biochemistry (Mosc)* **52**:7987–7998.
- Yuan S, Hu Z, Filipek S, and Vogel H (2015) W246(6.48) opens a gate for a continuous intrinsic water pathway during activation of the adenosine A2A receptor. *Angew Chem Int Ed Engl* **54**:556–559.
- Zacharias DA, Violin JD, Newton AC, and Tsien RY (2002) Partitioning of lipid-modified monomeric GFPs into membrane microdomains of live cells. *Science* **296**:913–916.
- Ziemek R, Brennauer A, Schneider E, Cabrele C, Beck-Sickinger AG, Bernhardt G, and Buschauer A (2006) Fluorescence- and luminescence-based methods for the determination of affinity and activity of neuropeptide Y2 receptor ligands. *Eur J Pharmacol* **551**:10–18.

FOOTNOTES

The financial support of the German Research Foundation [SFB1052/A3 and BE1264/16], the EU and Free State of Saxony [Grants 100148835 and 143213128452], and Max Kade Foundation is gratefully acknowledged.

FIGURE LEGENDS

Figure 1: Model of NPY bound to Y₂R, adapted from Kaiser et al. (2015) with modification. The peptide ligand (cyan) is accommodated deeply into the transmembrane bundle, with the side chain of Y³⁶ in close proximity to W^{6.48}. The rotameric state of W^{6.48} in the overlaid crystal structures of rhodopsin (pdb 1U19, palegreen) and NTSR1 (4GRV, sand) is given for comparison, and parts of TM4 are shown as ribbon for clarity.

Figure 2: Binding properties of wild type Y₂R and W^{6.48} mutants. Both saturation (A) and displacement binding (B) displayed wild type-like binding properties of W^{6.48} variants. (C) The receptor displayed two affinity states. High affinity ligand binding was stabilized by the G protein: Upon addition of GTP γ S to disrupt the high affinity R*G(empty) complex, maximal binding was reduced by increasing the portion of the fast phase of k_{off} while there was only one k_{on} in the concentration range of the radioligand tested. Accordingly, displacement experiments may be approximated using a two-site model (grey line). (D) This two-phase behavior in the dissociation kinetics indicative of two affinity states was also present in the W^{6.48} mutants, and could be modulated by the addition of GTP γ S in an analogous manner.

Data represent mean \pm SEM of at least three independent experiments each performed in duplicate. For clarity, in panels B-D each receptor variant was normalized to its own total (100%) and unspecific (0%) binding. 100% specific binding typically corresponded to about 1 fmol (WT Y₂R), 0.6 fmol (W^{6.48}Y), 0.8 fmol (W^{6.48}H; W^{6.48}T) ¹²⁵I-PYY. Numerical data and statistical evaluation can be found in Tab. 1.

Figure 3: Signaling of W^{6.48} mutants in second messenger assays. In (A), receptor response was redirected to the phospholipase C pathway using a chimeric G $\alpha_{\Delta 6qi4myr}$ in transiently transfected COS7 cells. Assays were normalized to maximal NPY stimulation of WT Y₂R (100%) and unstimulated cells (0%), the signal amplitude was dependent on transient transfection and varied between 15,000 dpm and 25,000 dpm (14-22fold over basal). (B), Concentration-response-curves obtained by a reporter gene assay downstream of the native

$G\alpha_i$ in transiently transfected HEK293. Mutation of $W^{6.48}$ shifted the EC_{50} , but hardly affected the apparent maximal signal. Assays were normalized to the forskolin-induced signal (100%) and full NPY inhibition (0%) of WT Y_2R , the signal amplitude was dependent on transient transfection and varied between 200 and 500 RLU (2-5fold over basal). Data represent mean \pm SEM of three independent experiments each performed in duplicate. Numerical data and statistical evaluation can be found in Tab. 2.

Figure 4: Arrestin3 recruitment and receptor internalization in living HEK293 cells. (A) Simulation of wild type Y_2R (depicted in yellow) leads to the recruitment of cytosolic arrestin3-mCherry (red) to the cell membrane for at least 30 min. Recruitment appeared more transient for $W^{6.48}Y$, and weaker for $W^{6.48}H/T$. Fluorescence intensity profiles along the grey lines in the merged pictures demonstrate the relocation of arrestin and co-localization with the receptor at the membrane. (B) After NPY stimulation, Y_2R -eYFP (depicted in yellow) and the $W^{6.48}Y$ mutant were rapidly internalized, which was reduced for $W^{6.48}H/T$ mutants. Live cell fluorescence microscopy with transiently transfected HEK293 cells, scale bar equals 10 μ m, nuclei stained with Hoechst33342 and depicted in blue. (C) Quantification of residual surface receptors after 60 min of agonist stimulation. All stimulated samples had significantly less receptors at the cell membrane compared to the control cells w/o stimulation. Compared to the wild type receptor, $W^{6.48}H/T$ internalized significantly weaker. Data analyzed by 2way ANOVA and Bonferroni's post test; * $p < 0.05$, ** $p < 0.01$, *** $p < 0.001$.

Figure 5: Y_2R -G-protein coupling studied by BRET. (A) and (C) display saturation BRET experiments of Y_2R -Rluc8 against gradients of $G\alpha_{i1}$ -Venus (A) and chimeric $G\alpha_{\Delta 6qi4myr}$ -Venus (C). For both types of $G\alpha$, there was significant and saturable BRET in the absence of ligand (open symbols) that was increased upon stimulation with 1 μ M NPY (closed symbols), indicative of a pre-assembled complex that changes its conformation upon activation (see text for details). This mechanism was preserved for $W^{6.48}$ mutants (bar graph). (B) and (D), ligand-dependent netBRET increase (recorded at saturating F/L ratio) was right-shifted for $W^{6.48}$

mutants, but E_{\max} was not reduced (except for $W^{6.48}H$, where saturation could not be reached up to 10 μM NPY). (E) Saturation BRET experiment for WT Y_2R and the control construct $G_{\alpha\Delta 6qmyr}$ -Venus lacking the C-terminal amino acids of $G_{\alpha_{i1}}$ (cf. panel G). Basal BRET was strongly reduced and no changes in the BRET signal was seen upon agonist stimulation. (F) All Venus-tagged G proteins were localized comparably in the plasma membrane. (G) N- and C-terminal sequences of the G_{α} -proteins used and sites for posttranslational modification. Data points represent mean \pm SEM of at least three independent experiments performed in quadruplicate. Numerical data and statistical evaluation can be found in Tab 3.

Figure 6: Y_2R -arrestin3 coupling studied by BRET. (A) Saturation BRET experiments of Rluc8-arrestin3 against a gradient of Y_2R -eYFP clearly show that interaction was only triggered by agonist stimulation, and was significantly reduced for $W^{6.48}$ mutants. (B) Concentration-response curves (recorded at saturating F/L ratio) were right-shifted for $W^{6.48}T$ and $W^{6.48}H$. (C) Reduced arrestin3 recruitment of $W^{6.48}$ mutants was not caused by slowed kinetics of arrestin3 interaction. Data points represent mean \pm SEM of at least three independent experiments performed in quadruplicate. Numerical data and statistical evaluation can be found in Tab 4.

Figure 7: Effects of modifications at position 36 of NPY on the activation/recruitment of $G_{\alpha_{i1}}$ (left panel), $G_{\alpha\Delta 6qi4myr}$ (middle), and arrestin3 (right). Ligand structures are given on the left. Activation was measured by ligand dependent BRET at saturating F/L ratio, and the curve of WT Y_2R /NPY for the respective pathway is indicated as dotted line for comparison. Stimulation with 1Nal³⁶-NPY, but not 2Nal³⁶-NPY, largely compensated signaling deficits of $W^{6.48}$ mutants, and was able to increase maximum arrestin3 recruitment. Data points represent mean \pm SEM of at least three independent experiments performed in quadruplicate. Numerical data and statistical evaluation can be found in Tab 5.

Figure 8: Suggested mechanism of effector coupling to the Y_2R . Inhibitory G proteins have a high affinity to the receptor even in the basal state, and are pre-assembled. Ligand binding

and activation of the receptor relocate W^{6.48}, and stabilize conformations with opened intracellular crevice, which enables G protein activation and recruitment of arrestin. Mutation of W^{6.48} to smaller amino acids interferes with this function as a bulky lever, but also alternative hydrogen bonding in the core of the receptor stabilize inactive conformations.

TABLES

Table 1: Binding properties of wild type and mutant Y₂R. Results of equilibrium as well as kinetic experiments are presented. W^{6.48} mutants displayed similar binding characteristics compared to wild type. A large difference between K_D and K_i in quasi-homologous binding experiments suggested the presence of two affinity states, which was corroborated by biphasic properties in k_{off} experiments. The presence of GTPγS shifted the population of these states, suggesting the high-affinity state to be G-protein dependent. All values are given as mean (95% confidence interval) corrected for multiple comparisons. Significance levels of K_D and logIC₅₀, respectively, relative to WT Y₂R were evaluated by 1way ANOVA followed by Dunnett's post test. Data for % fast phase +/- GTPγS were analyzed by 2way ANOVA and compared to the values in the absence of GTPγS by Bonferroni's post test. * p < 0.05; ** p < 0.01; *** p < 0.001; ns, not significant.

	Saturation binding ¹²⁵ I-PYY		Displacement binding (60 pM ¹²⁵ I- PYY/ NPY)		Dissociation rate k _{off}			
	K _D / pM	B _{max} / fmol mg ⁻¹	logIC ₅₀	logK _i	k _{off} – fast / min ⁻¹	k _{off} – slow / min ⁻¹	% fast	% fast +100 μM GTPγS
WT Y₂R	50 (7-93)	4329 (2802-5856)	-8.59 (8.74- 8.44)	-8.93 (9.08- 8.78)	0.41 (0.11-0.71)	0.0070 (0.0005- 0.0135)	35 (23-46)	60 * (42-78)
W^{6.48}Y	57 ^{ns} (0-120)	2614 (1386-3842)	-8.75 * (8.98- 8.53)	-9.06 (9.29- 8.84)	0.34 (0-0.75)	0.0066 (0-0.0160)	34 (12-56)	56 ^{ns} (26-86)
W^{6.48}H	40 ^{ns} (0-80)	2827 (1741-3913)	-8.37 * (8.50- 8.25)	-8.77 (8.89- 8.64)	0.18 (0-0.36)	0.0061 (0.0008- 0.0115)	15 (0-33)	52 ** (10-94)
W^{6.48}T	59 ^{ns} (10- 107)	3421 (2173-4669)	-8.62 ^{ns} (8.76- 8.48)	-8.93 (9.07- 8.78)	0.10 (0-0.20)	0.0052 (0-0.0148)	28 (0-58)	77 *** (45-100)

Table 2: Receptor signaling in second messenger assays conducted with either chimeric $G_{\alpha_{\Delta 6qi4myr}}$ protein or native G_i . Mutation of $W^{6.48}$ mainly altered potency but not efficacy (E_{max}). Curves were analyzed with the classic logistic function (columns 1 and 2) and the operational model of agonism (columns 3-5). The efficacy term τ was corrected to the surface expression of each construct to retrieve τ_c . Hill slope was set to unity for both analyses. All values are given as mean (95% confidence interval) corrected for multiple comparisons. Significance levels of $\log(\tau_c/K_A)$ relative to WT Y_2R were evaluated by 1way ANOVA followed by Dunnett's post test. * $p < 0.05$; ** $p < 0.01$; *** $p < 0.001$; ns, not significant.

	3H -IP (via $G_{\alpha_{\Delta 6qi4myr}}$)					cAMP (via G_{α_i})				
	logEC ₅₀	E _{max} / %	log τ_c	logK _A	log (τ_c/K_A)	logEC ₅₀	E _{max} / %	log τ_c	logK _A	log (τ_c/K_A)
WT Y₂R	-9.48 (9.22-9.74)	100	1.466 (0.927-2.005)	-8.02 (9.07-6.96)	9.48 (9.32-9.65)	-10.67 (11.25-10.09)	100	1.63 (-0.83-4.08)	-9.04 (11.66-6.41)	10.66 (10.22-11.10)
W^{6.48}Y	-8.70 (8.39-9.01)	91 (80-102)	1.153 (0.895-1.411)	-7.87 (8.40-7.33)	9.02 * (8.75-9.28)	-10.06 (10.60-9.52)	90 (65-114)	1.26 (0.60-1.91)	-9.08 (9.93-8.24)	10.34 ns (9.85-10.83)
W^{6.48}H	-7.94 (7.94-8.83)	89 (72-106)	0.758 (0.344-1.172)	-7.59 (8.35-6.83)	8.35 *** (7.85-8.85)	-9.46 (10.26-8.67)	79 (50-108)	0.52 (-0.16-1.20)	-8.80 (9.76-7.84)	9.32 *** (8.51-10.12)
W^{6.48}T	-8.43 (8.01-8.85)	85 (70-100)	0.822 (0.444-0.998)	-7.80 (8.39-7.22)	8.52 *** (8.11-9.93)	-9.53 (10.24-8.83)	89 (60-117)	1.13 (-0.05-2.32)	-8.50 (9.89-7.10)	9.63 ** (8.98-10.29)

Table 3: Saturation BRET of Y₂R-Rluc8 variants with G α_{i1} - and G $\alpha_{\Delta 6q14myr}$ -Venus. BRET of wild type and mutant receptors were analyzed against a gradient of G protein, with and without ligand stimulation. Significant and saturable BRET was present also in the absence of NPY, suggesting pre-assembly of the complex. NPY stimulation increased total BRET, but half maximal signal occurred at similar F/L ratios (BRET₅₀), indicative of structural re-organization rather than additional recruitment upon NPY activation. This mechanism was preserved for the W^{6.48} variants. However, stimulation with 1 μ M was not sufficient to induce WT-like netBRET of W^{6.48} mutants with G $\alpha_{\Delta 6q14myr}$ -Venus (*cf.* EC₅₀ values of activation in Tab. 5). All values are given as mean (95% confidence interval) corrected for multiple comparisons. Statistical significance of netBRET changes relative to the WT Y₂R was assessed by 1wayANOVA and Dunnett's post test. * p < 0.05; ** p < 0.01; *** p < 0.001; ns, not significant.

	G α_{i1} -Venus					G $\alpha_{\Delta 6q14myr}$ -Venus				
	unstimulated		stimulated 1 μ M NPY			unstimulated		stimulated 1 μ M NPY		
	BRET ₅₀	max. BRET	BRET ₅₀	max. BRET	netBRET	BRET ₅₀	max. BRET	BRET ₅₀	max. BRET	netBRET
WT Y₂R	0.007 (0.005-0.009)	0.189 (0.171-0.206)	0.009 (0.007-0.012)	0.245 (0.220-0.271)	0.046 (0.038-0.0587)	0.012 (0.0028-0.028)	0.081 (0.064-0.098)	0.010 (0.006-0.014)	0.122 (0.107-0.136)	0.034 (0.027-0.041)
W^{6.48} Y	0.007 (0.0014-0.014)	0.156 (0.119-0.192)	0.010 (0.001-0.019)	0.194 (0.160-0.230)	0.039 ^{ns} (0.008-0.069)	0.012 (0.0029-0.029)	0.126 (0.091-0.161)	0.008 (0.0019-0.019)	0.138 (0.106-0.169)	0.014 ^{**} (0.003-0.025)
W^{6.48} H	0.008 (0.004-0.012)	0.206 (0.175-0.237)	0.010 (0.006-0.015)	0.257 (0.222-0.292)	0.042 ^{ns} (0.034-0.050)	0.007 (0.0017-0.017)	0.099 (0.068-0.130)	0.009 (0.0023-0.023)	0.101 (0.064-0.139)	0.003 ^{***} (-0.015-0.022)
W^{6.48} T	0.007 (0.003-0.010)	0.170 (0.140-0.200)	0.008 (0.004-0.012)	0.226 (0.188-0.264)	0.040 ^{ns} (0.023-0.056)	0.006 (0.0013-0.013)	0.071 (0.048-0.094)	0.007 (0.0015-0.015)	0.094 (0.062-0.126)	0.020 [*] (0.002-0.038)

Table 4: Saturation BRET of Y₂R-eYFP with Rluc8-arrestin3 and kinetic parameters of recruitment. BRET of wild type and mutant receptors were analyzed against an arrestin3 gradient (columns 1 and 2). Detectable BRET only occurred upon NPY stimulation, and maximal arrestin3 recruitment was significantly reduced for the W^{6,48} variants. Kinetic profiles of recruitment (columns 3 and 4) recorded at saturating F/L ratios specify that this was not due to slowed complex formation. All values are given as mean (95% confidence interval) corrected for multiple comparisons. Statistical significance of netBRET changes relative to the WT Y₂R was assessed by 1wayANOVA and Dunnett's post test. *** p < 0.001.

	Arr3-Rluc recruitment, 1 μM NPY			10 μM NPY
	BRET ₅₀	netBRET	K _{obs} / min ⁻¹	K _{obs} / min ⁻¹
WT Y₂R	0.0011 (0.0005-0.0017)	0.429 (0.384-0.474)	0.286 (0.210-0.362)	0.292 (0.234-0.351)
W^{6,48}Y	0.0020 (0-0.0045)	0.241 (0.137-0.345) ***	0.618 (0.391-0.845)	0.518 (0.232-0.805)
W^{6,48}H	0.0044 (0.0004-0.0084)	0.176 (0.100-0.251) ***	0.357 (0.233-0.480)	0.323 (0.219-0.427)
W^{6,48}T	0.0022 (0.007-0.0037)	0.222 (0.161-0.283) ***	0.452 (0.258-0.645)	0.391 (0.271-0.511)

Table 5:

Effects of modifications at position 36 of NPY on the binding affinity and activation of different pathways. Binding affinities were determined in displacement binding experiments (*cf.* Tab. 1). Activation was measured by ligand-dependent increase of the BRET ratio for the respective effector ($G\alpha_{i1}$, $G\alpha_{\Delta 6qj4myr}$, arrestin3) at saturating F/L ratio. Stimulation with $1\text{NaI}^{36}\text{-NPY}$, but not $2\text{NaI}^{36}\text{-NPY}$, largely compensated signaling deficits of $W^{6.48}$ mutants, and was able to increase maximum arrestin3 recruitment. Both, results from classic sigmoidal (logistic) fit and transduction coefficient from operational model of agonism are given, with Hill slope set to unity for all analyses, and values are given as mean (95% confidence interval) corrected for multiple comparisons. Significance levels of $\log\text{IC}_{50}$ and $\log(\tau/K_A)$, respectively, were evaluated by 2way ANOVA and Bonferroni's post test for each mutant relative to the WT Y_2R treated with the same peptide. * $p < 0.05$; ** $p < 0.01$; *** $p < 0.001$; ns, not significant.

	Displacement binding (60 pM ^{125}I -PYY)		Ligand-dependent BRET										
	$\log\text{IC}_{50}$	x-fold over WT	$G\alpha_{i1}$			$G\alpha_{\Delta 6qj4myr}$			Arrestin3				
			$\log\text{EC}_{50}$	x-fold over WT/NPY	$\log(\tau/K_A)$	$\log\text{EC}_{50}$	x-fold over WT	$\log(\tau/K_A)$	$\log\text{EC}_{50}$	x-fold over WT	netBRET	% WT	$\log(\tau/K_A)$
NPY													
WT Y_2R	-8.59 (8.74-8.44)	(1)	-8.50 (8.91-8.10)	(1)	8.39 (8.07-8.72)	-7.42 (7.87-6.98)	(1)	7.33 (6.99-7.67)	-7.12 (7.21-7.02)	(1)	0.51 (0.48-0.53)	(100)	7.15 (7.08-7.21)
$W^{6.48}Y$	-8.75 ns (8.98-8.53)	1	-7.99 (8.50-7.48)	5	7.95 ns (7.45-8.45)	-6.79 (7.44-6.14)	4	6.81 * (6.39-7.23)	-7.08 (7.23-6.92)	1	0.28 (0.25-0.30)	55	6.80 * (6.69-6.91)
$W^{6.48}H$	-8.37 * (8.50-8.25)	1	-7.11 (-7.57-6.65)	30	7.17 *** (6.71-7.63)	> -5.70 a	> 50	5.49 *** (4.63-6.36)	-6.01 (6.14-5.89)	13	0.25 (0.23-0.28)	49	5.72 *** (5.59-5.84)
$W^{6.48}T$	-8.62 ns (8.76-8.48)	1	-7.35 (7.71-6.98)	18	7.43 *** (7.07-7.80)	-6.14 (6.72-5.55)	20	6.04 *** (5.56-6.53)	-6.44 (6.54-6.33)	5	0.26 (0.24-0.27)	51	6.13 *** (6.02-6.25)
$1\text{NaI}^{36}\text{-NPY}$													
WT Y_2R	-8.41 (8.66-8.16)	1	-8.18 (9.11-7.25)	2	8.05 (7.42-8.67)	-6.93 (7.46-6.41)	3	6.88 (6.46-7.30)	-7.08 (7.25-6.92)	1	0.46 (0.42-0.50)	90	7.02 (6.90-7.13)

W^{6.48} Y	-8.58 ns (8.84- 8.32)	1	-7.91 (8.86- 6.95)	5	7.84 ns (7.18 - 8.49)	-6.74 (7.38- 6.09)	5	7.11 ns (6.71 - 7.52)	-7.41 (7.57- 7.25)	0.5	0.26 (0.24- 0.28)	51	7.10 ns (6.89 - 7.31)
W^{6.48} H	-9.45 *** (9.61- 9.29)	0.1	-7.79 (8.66- 6.93)	6	7.64 ns (6.88 - 8.39)	-6.47 (7.01- 5.92)	9	6.24 ** (5.71 - 6.78)	-7.00 (7.14- 6.86)	1	0.36 (0.33- 0.39)	71	6.85 ns (6.70 - 7.00)
W^{6.48} T	-9.22 *** (9.43- 9.01)	0.2	-8.05 (8.81- 7.30)	3	8.04 ns (7.32 - 8.76)	-6.56 (7.18- 5.94)	8	6.57 ns (6.12 - 7.02)	-7.18 (7.28- 7.09)	1	0.39 (0.37- 0.40)	76	7.06 ns (6.92 - 7.20)
2NaI³⁶-NPY													
WT Y₂R	-8.10 (8.39- 7.82)	2	-8.13 (8.84- 7.42)	4	8.23 (7.75 - 8.71)	-6.74 (7.41- 6.07)	5	6.63 (6.18 - 7.09)	-7.02 (7.16- 6.89)	1	0.41 (0.38- 0.44)	80	6.90 (6.75 - 7.05)
W^{6.48} Y	-8.28 ns (8.52- 8.04)	2	-7.98 (8.81- 7.16)	5	8.01 ns (7.53 - 8.49)	-6.53 (7.07- 6.00)	8	6.59 ns (6.19 - 6.99)	-7.00 (7.16- 6.83)	1	0.26 (0.24- 0.28)	51	6.67 ns (6.44 - 6.90)
W^{6.48} H	-8.14 ns (8.41- 7.87)	3	-7.09 (7.52- 6.65)	38	6.97 *** (6.48 - 7.47)	> -6.00 a	> 25	5.92 ** (5.20 - 6.65)	-6.30 (6.46- 6.15)	7	0.17 (0.15- 0.18)	33	5.78 *** (5.39 - 6.17)
W^{6.48} T	-8.11 ns (8.47- 7.76)	3	-7.16 (7.81- 6.51)	26	7.08 *** (6.54 - 7.63)	> -6.00 a	> 25	5.70 *** (4.92 - 6.49)	-6.60 (6.95- 6.25)	3	0.06 (0.05- 0.07)	12	5.73 *** (4.66 - 6.79)

^a curves do not reach saturation

FIGURES

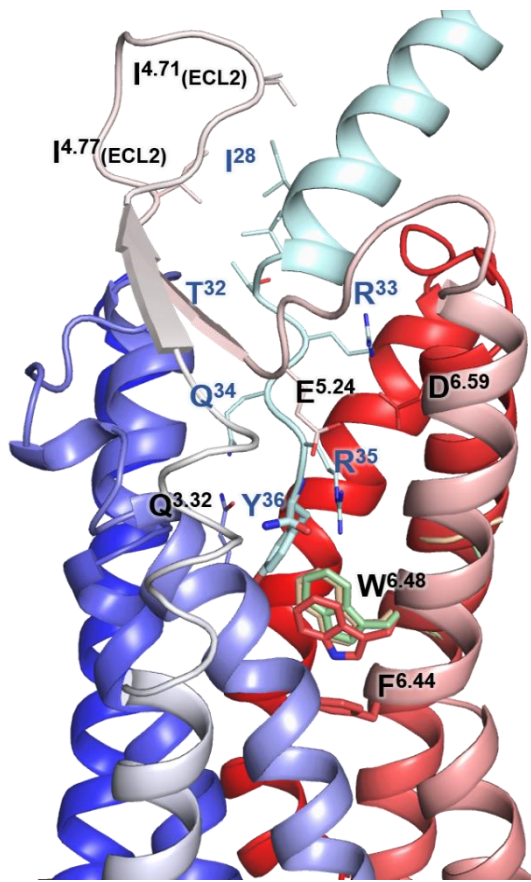


Figure 1

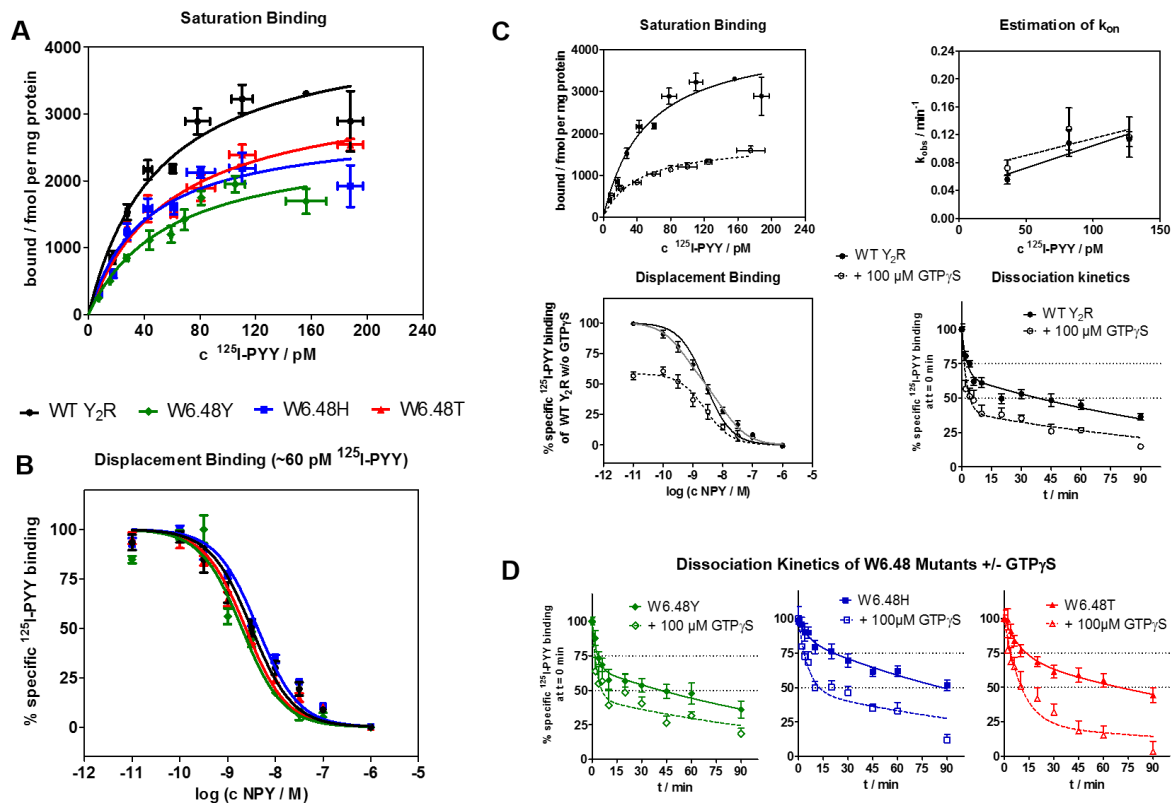


Figure 2

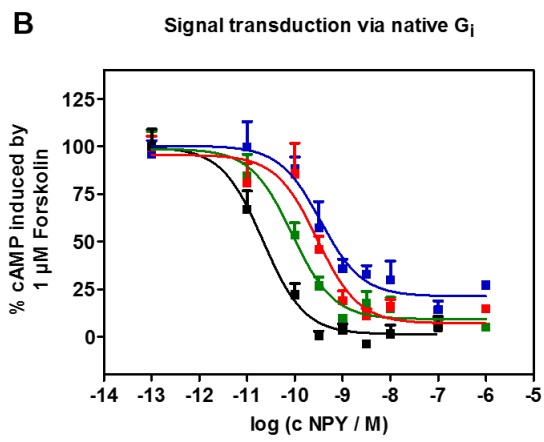
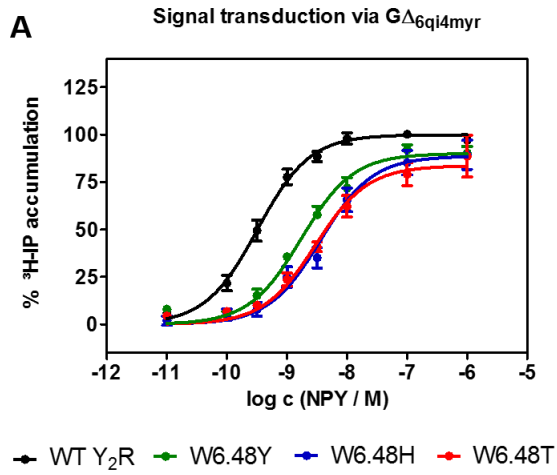


Figure 3

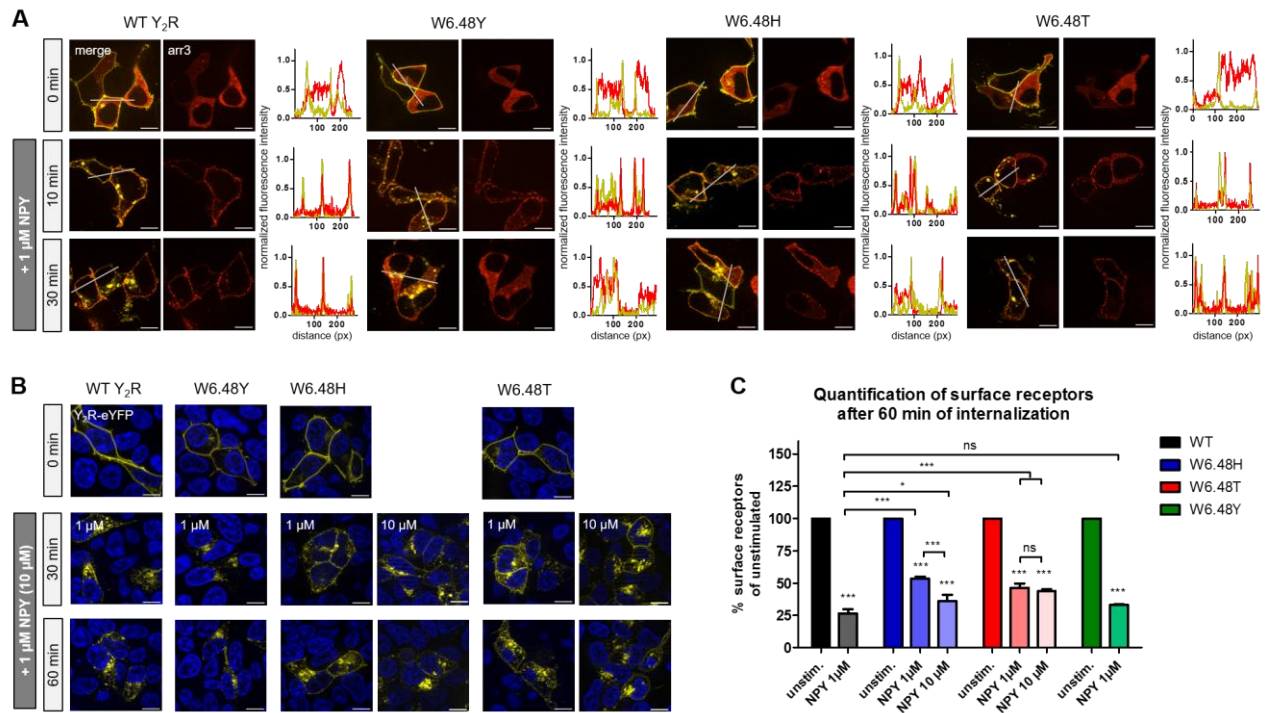


Figure 4

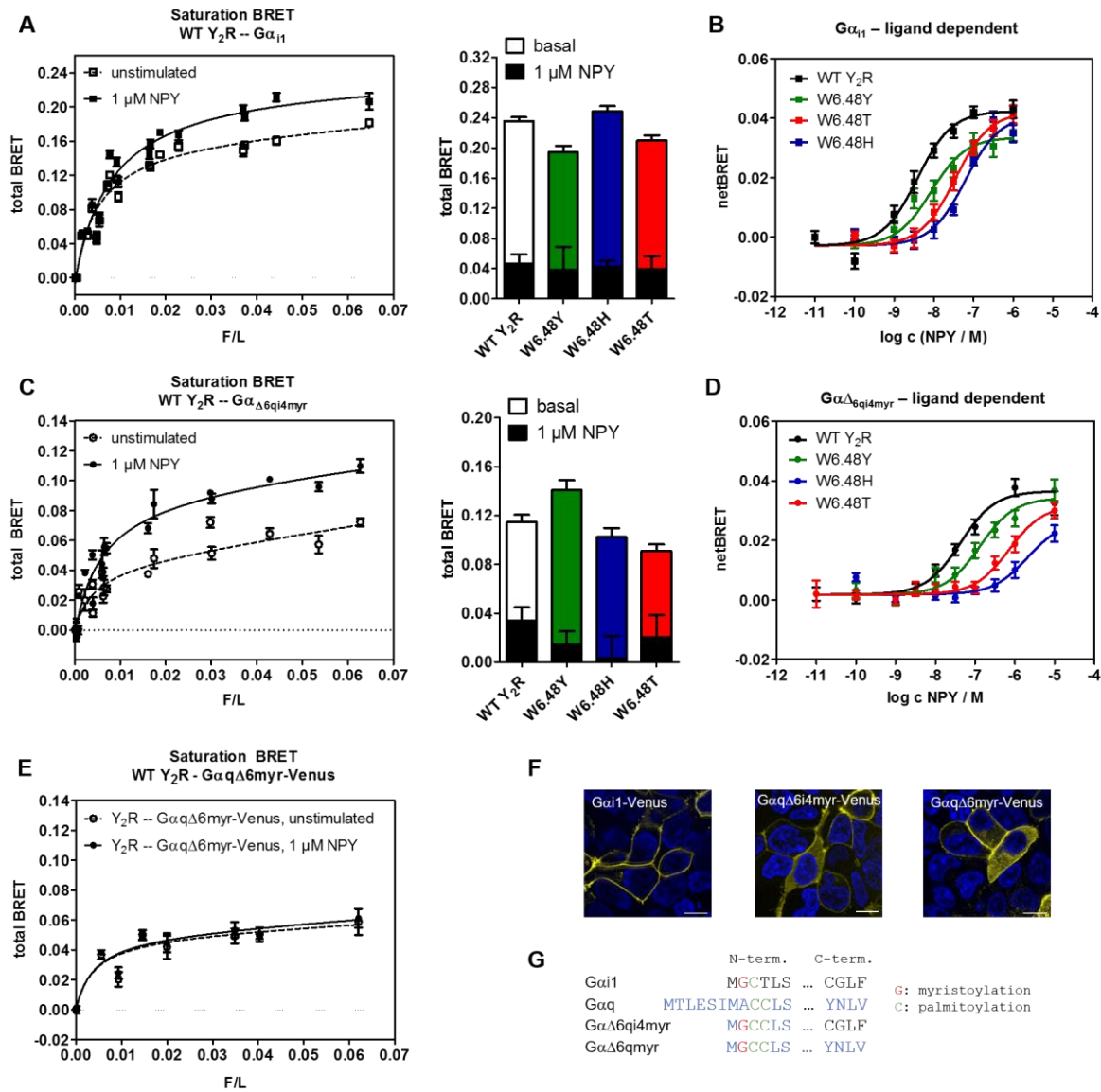


Figure 5

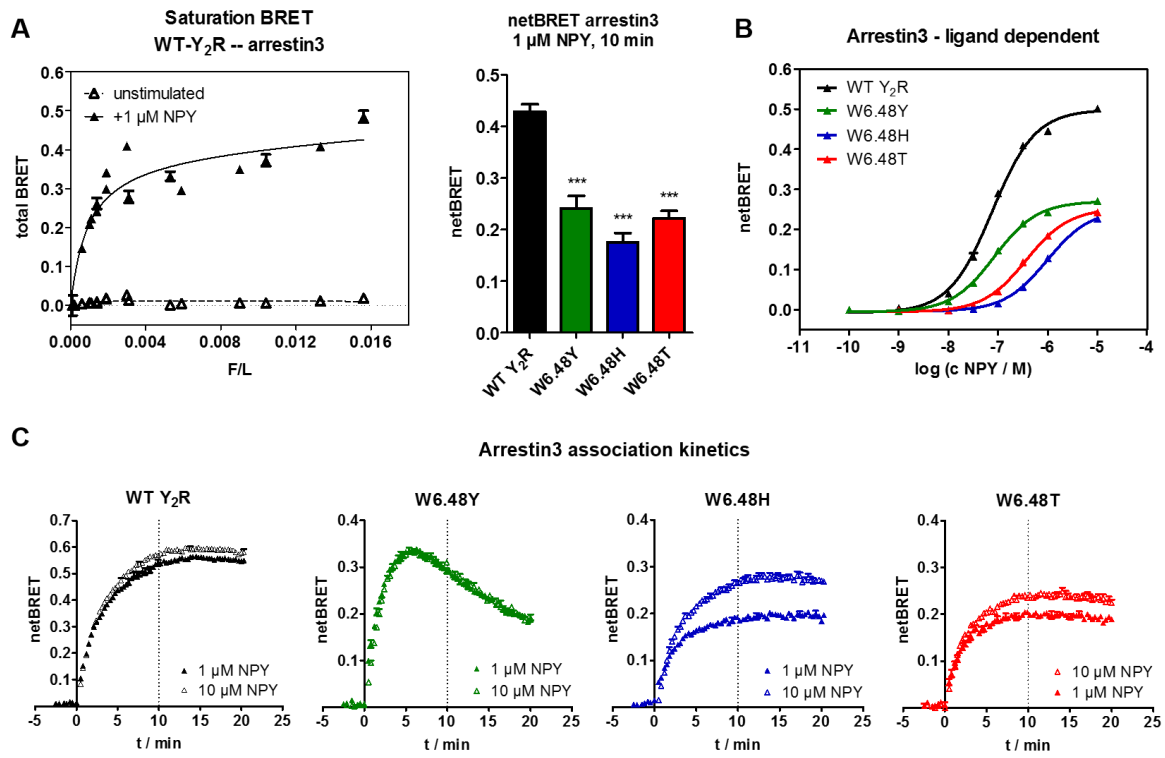


Figure 6

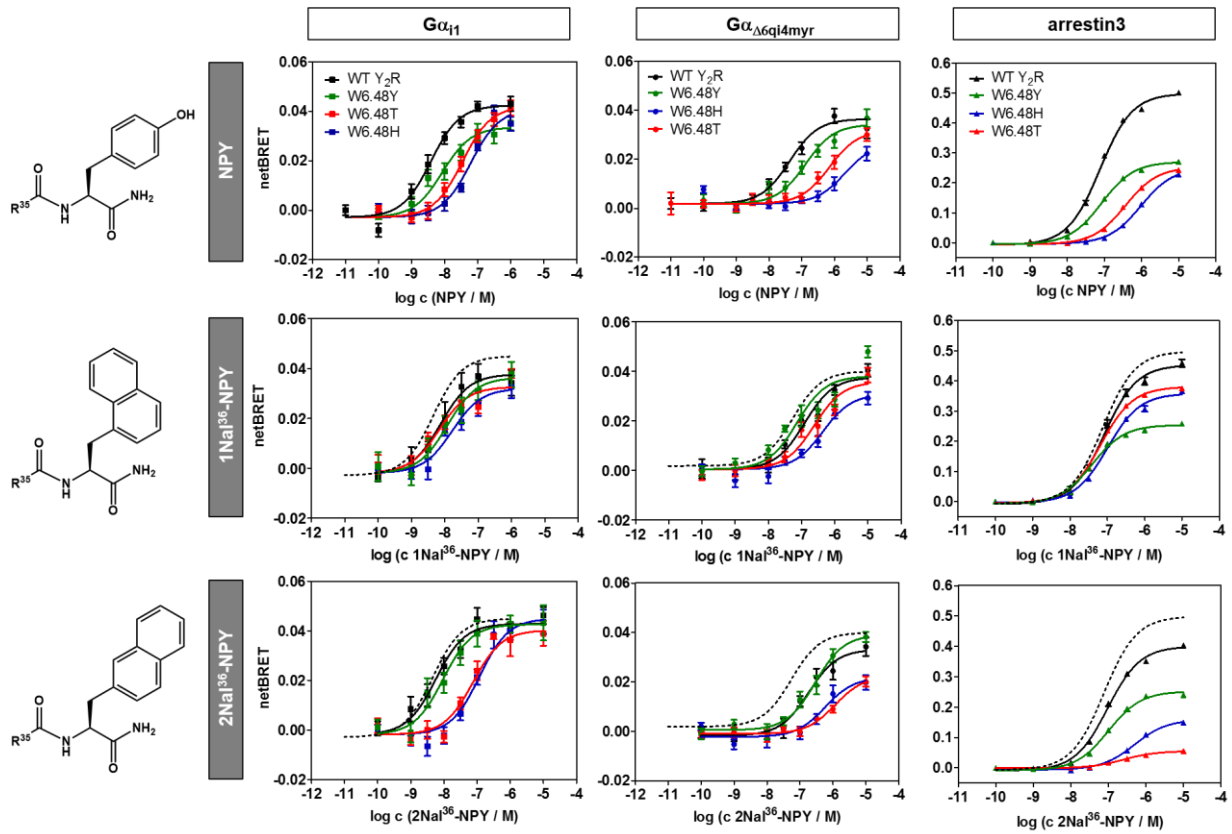


Figure 7

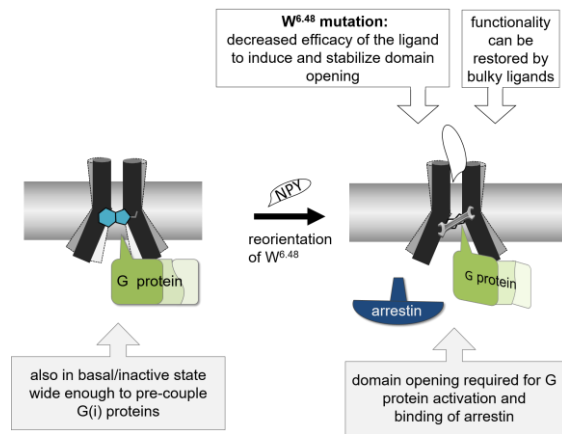


Figure 8